Structured Light from Classical to Quantum Perspectives

Bokić, Bojana; de Coene, Yovan; Ferrara, Maria Antonietta; Verbiest, Thierry; Caudano, Yves; Kolaric, Branko

Published in:
Symmetry

DOI:
10.3390/sym16081053

Publication date:
2024

symmetry

MDPI

Perspective

Structured Light from Classical to Quantum Perspectives

Bojana Bokić [1], Yovan de Coene [2], Maria Antonietta Ferrara [3], Thierry Verbiest [2], Yves Caudano [4] and Branko Kolaric [1,5,*]

1 Nanophotonics Laboratory, Photonics Center, Institute of Physics, University of Belgrade, Pregrevica 118, 11080 Belgrade, Serbia; bojana@ipb.ac.rs
2 Molecular Imaging and Photonics, Department of Chemistry, KU Leuven, Celestijnenlaan 200 D, Box 2425, B-3001 Leuven, Belgium; yovan.decoene@kuleuven.be (Y.d.C.); thierry.verbiest@kuleuven.be (T.V.)
3 Institute of Applied Sciences and Intelligent Systems, Unit of Naples, National Research Council, Via Pietro Castellino 111, 80131 Naples, Italy; antonella.ferrara@na.isasi.cnr.it
4 Department of Physics & Namur Institute of Structured Matter (NISM) and Namur Institute for Complex Systems (naXys), University of Namur, Rue de Bruxelles 61, B-5000 Namur, Belgium; yves.caudano@unamur.be
5 Micro- and Nano-Photonics Materials Group, University of Mons, Avenue Maistriau 19, B-7000 Mons, Belgium
* Correspondence: branko.kolaric@umons.ac.be

Abstract: Most optical phenomena result from the interaction of electromagnetic waves with matter. However, the light structure can be eminently more complex than plane waves, with many degrees of freedom and dimensions involved, yielding intricate configurations. Light transcends the conventional landscape of electromagnetism, offering the possibility to tailor light in three dimensions (intermixing all three electric field components), in four-dimensional spacetime (for fields manifesting both temporal and spatial patterns), and, beyond that, to make structured quantum light, tuning its characteristics at an unprecedented new level of control. This article addresses the physical foundations of structured light, its interactions with matter, including the nonlinear regime and probing chirality, its classical benefits with holography as a specific highlight, and quantum mechanical applications. It describes the various applications connecting structured light with material physics, quantum information, and technology. Notably, we discuss weak measurements with structured light acting as the meter with connections to probing structured-light beam shifts at interfaces. Ultimately, revealing the interplay between structured light and matter opens attractive avenues for different new technologies and applications, covering both the classical and the quantum realms.

Keywords: structured light; chirality; holography; weak measurements; quantum applications

Citation: Bokić, B.; de Coene, Y.; Ferrara, M.A.; Verbiest, T.; Caudano, Y.; Kolaric, B. Structured Light from Classical to Quantum Perspectives. *Symmetry* **2024**, *16*, 1053. https://doi.org/10.3390/sym16081053

Academic Editor: Alberto Ruiz Jimeno

Received: 17 May 2024
Revised: 1 July 2024
Accepted: 12 July 2024
Published: 15 August 2024

1. Introduction

The new science that was born at the beginning of the 20th century aims to describe a microscopic reality that cannot be sufficiently and correctly described by classical physics. New ideas, such as the postulate of quantization of energy and the concept of the photon (carrier of the energy of the electromagnetic field), were introduced and led to the development of the new theory known today as Quantum Mechanics. Through the concept of the photon [1], as a quantum of oscillating electromagnetic field, the new physics of light emerged, connecting the corpuscular and electromagnetic wave nature of light in a single unity. Also, with the development of new physics, topology has become not only a fundamental branch of mathematics but also a tool that connects advanced mathematical concepts of space and its transformations with the physics and dynamics of physical systems. In this account, we are especially interested in describing the link between the shape and geometry of electromagnetic waves with their properties [2,3]. Complex structured light shows great potential in that regard [4,5]. That makes ideas issued from the field of topology relevant to other disciplines, such as chaos, continuum mechanics, nonlinear

dynamics, electromagnetism, quantum physics, mathematical biology, and physics of communication, to give a few examples. It should be emphasized that the vector nature of light (polarization, vector potential, vectorial fields, etc.) is indispensable in describing light-matter interactions in various systems and controls numerous phenomena, such as diffraction, scattering, nonlinear processes, and polarization-sensitive interactions [6]. Now, we acquired the capability to design and shape the polarization of optical beams from high to low intensities, down to the single-photon level. Subsequently, that enabled the study of topological phenomena. These advancements also went along increased control of phase and polarization singularities, as well as of orbital angular momentum (OAM) of light and spin angular momentum (SAM) [2,7], including spin-orbit coupling. It also spurred progress in areas as diverse as optical sensors and spectroscopy, holography, ellipsometry, nonlinear optics, and super-resolution imaging. Furthermore, vectorial light fields provide us with more informational resources than homogeneously polarized plane waves. Indeed, while classical, these fields exhibit nonseparable properties, evidenced through correlations reminiscent of quantum entanglement. In addition to applications, the concept of structured light uniquely connects the shape and geometry of light waves with matter [8].

In this account, we first briefly introduce structured light with a detailed description of a few attractive beams (diffracting and nondiffracting) for photonics and material applications, focusing mainly on the applications of structured light in spectroscopy, chirality, and quantum studies. Subsequently, we also summarized structural light in prominent applications such as linear and nonlinear photonics and holography. In the end, we present the applications of structured light from the quantum perspective, highlighting the power of structured light for fundamental quantum studies and applications relevant to quantum technologies, including the context of quantum weak measurements. This article is aimed at the broad community of physicists, quantum researchers, and physical chemists, with the goal of attracting attention to structured light and its applications in material and quantum science. It serves as a first step in enlightening these communities about the unusual properties of electromagnetic waves, which differ significantly from simple plane waves, and their vast potential for fundamental control of light-matter interaction, as well as applications in material and communication sciences. With that respect, we highlighted original applications, which we believe are of particular interest for these communities, and which were not the focus of previous reviews on structured light (such as probing chirality, holographic applications, and quantum weak measurements, to cite a few).

2. Structured Light: Nondiffracting and Accelerating Beams

Commonly, electromagnetic wave fields undergo diffraction during propagation, resulting in a transverse spreading of the field distribution. However, there are beam classes that maintain their profile along propagation. Such beams became famous as diffraction-free or nondiffracting beams [9]. Nondiffracting beams were first introduced by Durnin in 1987 [10], as monochromatic optical fields with propagation-invariant transverse intensity distributions. Mathematically, they are particular solutions of the Helmholtz equation

$$\partial_t^2 U(x,y) + k_t^2 U(x,y) = 0. \quad (1)$$

in different coordinate systems: Cartesian, circular cylindrical, elliptical cylindrical, and parabolic cylindrical coordinates [11,12]. Such coordinate systems give rise to a certain type of nondiffracting beam: discrete (plane wave and their superpositions) [11], Bessel [13], Mathieu [14], and Parabolic beams [15], respectively.

Nondiffracting beams have been studied in different configurations. Two-dimensional periodic intensity patterns can be generated as a superposition of multiple plane waves [11], but a quasiperiodic pattern such as a Penrose lattice is generated as a superposition of five plane waves [16]. Bessel beams are obtained by solving the Helmholtz equation in circular cylindrical coordinates and their transverse intensity distributions are characterized by concentric rings; Figure 1a depicts a Bessel beam. They possess a whole class of higher-order modes, which are typically indicated by one integer. Additionally, their higher-

order modes carry optical orbital angular momentum (OAM) along their propagation axis, which can be transferred to trapped particles. Bessel beams can be easily generated with conical lenses, so-called axicons, and they are the most investigated [17]. In recent studies, Bessel beams have been used to induce periodic photonic lattices [12], and even Fibonacci photonic lattices [18]. Bessel beams are already well described and reviewed as the simplest form of light with OAM after the Laguerre–Gauss beams. In this highlight, we focus more on other types of structured beams (Airy, Matthieu, and Laguerre–Gauss) and their applications in spectroscopic and quantum studies that could be exploited in various optical and quantum technologies. A third family of nondiffracting beams, so-called Mathieu beams, are solutions of the Helmholtz equation in elliptical symmetry. The transverse intensity distribution of Mathieu beams consists of discrete spots along elliptic or hyperbolic paths; one example is shown in Figure 1b. Their generation is more complicated, compared to Bessel beam generation as there are no commercially available simple refractive devices. One option for their realization is the holographic generation with spatial light modulators (SLM). A nondiffracting beam that is distorted by an obstacle within the beam path reconstructs its original transverse shape after a distinct propagation length. This feature makes nondiffracting beams highly suited for three-dimensional applications. Moreover, helical Mathieu beams that are superpositions of even and odd modes of Mathieu beams, provide continuous phase variations, so they have been used to investigate the transfer of orbital angular momentum to particles in optical micromanipulation [9,19].

Parabolic beams are the fourth family of nondiffracting beams, they are a solution of the Helmholtz equation in the parabolic cylindrical coordinate system and might be interesting for further applications in optical micromanipulation. One intensity distribution of the Parabolic beam is depicted in Figure 1c.

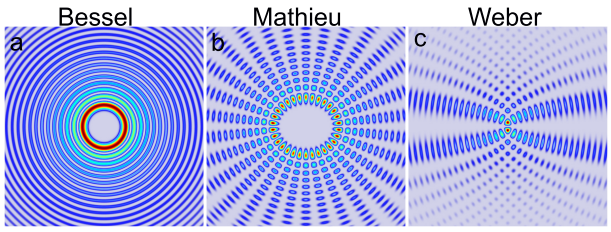

Figure 1. Typical examples of nondiffracting beams: transverse field distributions of selected (**a**) Bessel, (**b**) Mathieu, and (**c**) Weber beams.

Nondiffracting beams with finite energy are bounded by the homogeneously transmitting aperture of finite dimensions or by the Gaussian aperture, and they are known as pseudo-nondiffracting beams. Experimental and numerical investigations show that the nondiffracting and pseudo-nondiffracting beams have δ-like angular spectrum, represented by a circle in the Fourier plane, that confirms their propagation-invariant character making such beams useful in optical micromanipulation, wireless communication and nonlinear optics [20,21].

Apart from eliminating diffraction, additional properties of such beams are observed, that make them useful for potential applications. One of them is the robustness of the nondiffracting beams: they show resistance against both amplitude and phase distortions, and they are able to regenerate themselves to the original form in the free propagation behind a nontransparent obstacle [22,23]. Nondiffracting beams also possess a self-reconstruction ability [24]. Well-known methods of generating nondiffracting beams require the use of the computer-generated holograms [25], the axicon [26] or the programmable spatial light modulators [27].

2.1. Applications of Accelerating Beams

Since their revelation by Berry and Balazs, the appealing class of Airy beams has attracted vast interest in different fields of physics. Originally, Airy beams were introduced as wave functions, solving the one-dimensional Schrödinger equation for free particles. Their probability density exceptionally stays non-spreading under time evolution, while

being transversely accelerated to follow a parabolic trajectory [28]. Due to the formal equivalence between the Schrödinger equation in quantum mechanics and the paraxial equation of diffraction in optics, the concepts and solutions can be exploited within the field of optics, where Airy beams can be directly observed and revealed in experiments [29,30].

They are invariant along parabolic trajectories and attract enormous attention because of their unique properties. Contrary to the previously mentioned straight nondiffracting beams, they belong to the class of accelerating nondiffracting beams and propagate on curved trajectories. Figure 2 shows the transverse (a) and longitudinal (b) intensity distribution of a two-dimensional Airy beam.

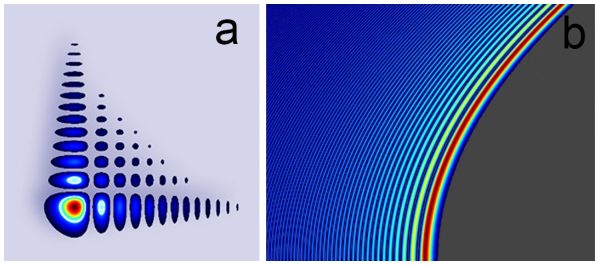

Figure 2. Two-dimensional Airy beam: Numerical simulation of (**a**) transverse intensity distribution, and (**b**) the intensity distribution along the propagation.

Their transverse self-acceleration [31,32] and nondiffraction [33,34] features make them useful for various applications ranging from laser micromachining (Figure 3a) [35], ultra-fast self-accelerating pulses [36] to dynamically routing surface plasmon polaritons (Figure 3b) [37,38], self-bending plasma channels (Figure 3c) [39], and frequency generation [40]. In optical micromanipulation, they have been proposed as an "optical snowblower" (Figure 3d) due to their ability of two-dimensional particle transport [20]. Their special self-healing properties and self-reconstruction after passing small obstacles have been demonstrated theoretically and experimentally [41].

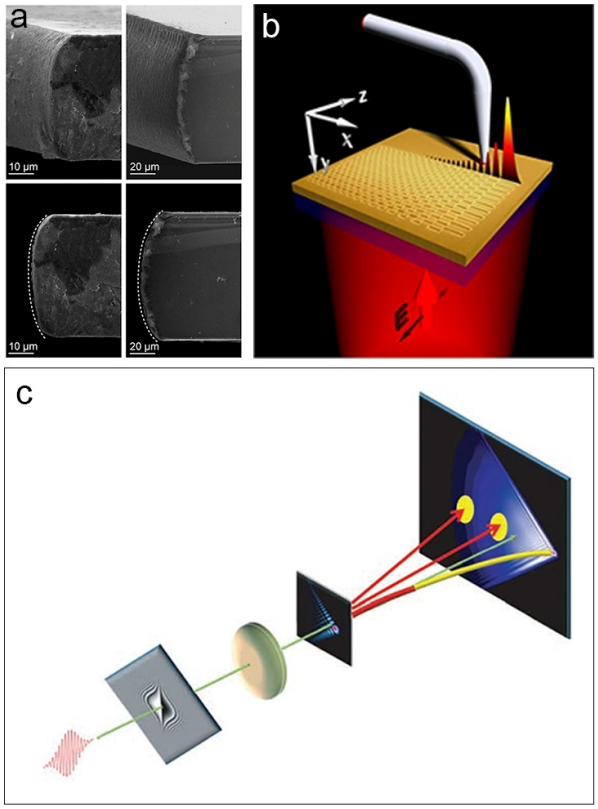

Figure 3. *Cont.*

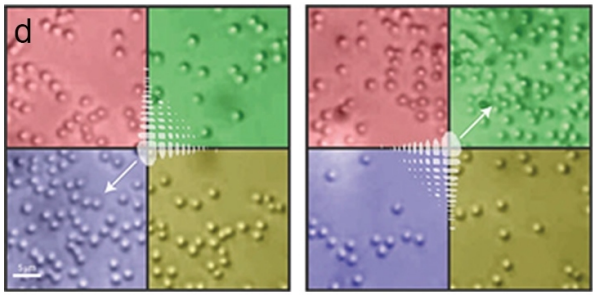

Figure 3. Applications with Airy beams: (**a**) Femtosecond laser micromachining with accelerating beams in diamond (left) and silicon (right), top row represents 3D view images of the samples while bottom row shows the same samples but with a profile orientation—Reprinted from [35], with the permission of AIP Publishing, (**b**) generation of Airy plasmons (scheme of the experimental set-up)—Reprinted figure with permission from [38], ©2011 by the American Physical Society, (**c**) curved plasma channel generation (scheme of the experimental set-up) From [39]—Reprinted with permission from AAAS, and (**d**) optically mediated particle clearing, micrographs of the colloids exposed to the Airy beam with two different rotations (left and right) of the beam [20]—Reproduced with permission from SNCSC.

2.2. *Applications of Nondiffracting Beams*

The science of nondiffracting beams carries great potential and is well-recognized for advancing many fields, especially in discrete and nonlinear photonics [42–44]. Some examples considering Airy beams are the influence of photonic lattice or refractive index gradient to control or compensate the Airy beam self-acceleration and design the beam caustics itself [42–47], as well as using two-dimensional Airy beams to optically induce light-guiding structures for various applications such as optical signal routing and switching [48].

The effects of nonlinearity on Airy beam propagation have been investigated in many theoretical and experimental studies [49–51]. Nonlinearity added a new degree of freedom to the system leading to interesting effects and phenomena. One of the well-known and most fundamental effects in nonlinear systems is the existence of spatial solitons—localized structures that preserve their shape owing to the balance between diffraction and nonlinear self-focusing. Arising from the interaction of multiple two-dimensional Airy beams in a nonlinear medium, a new type of soliton formation has been demonstrated [52]. Depending on different phase configurations of such synthesized beams (in phase or out of phase), either one solitary solution (Figure 4a) or a pair (Figure 4b) is observed that propagates almost stable with small intensity modulations (breathing).

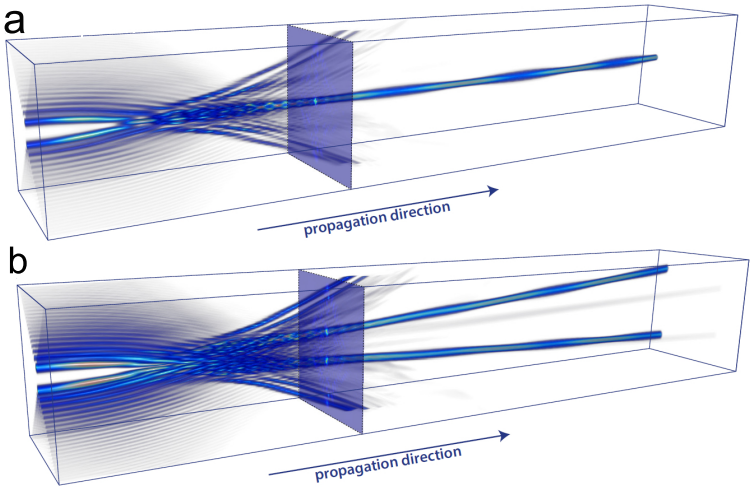

Figure 4. Formation of solitary states from the interaction of two Airy beams: (**a**) in-phase, and (**b**) out-of-phase. Reprinted with permission from [52] © Optica Publishing Group.

Another class of nondiffracting beams, Mathieu beams, are mostly used as lattice-writing light to fabricate discrete waveguide structures and investigate their nonlinear self-action, which lead to the morphing of the discrete diffraction [53]. It is linked to linear discrete diffraction with nonlinear self-effects and demonstrates a gradual transition from one to two dimensions (Figure 5). Discrete diffraction similar to the typical one observed in 1D waveguide arrays is demonstrated with Mathieu beams of zeroth order propagating in nonlinear media (Figure 5a). With higher-order Mathieu beams, discrete diffraction is observed along each layer.

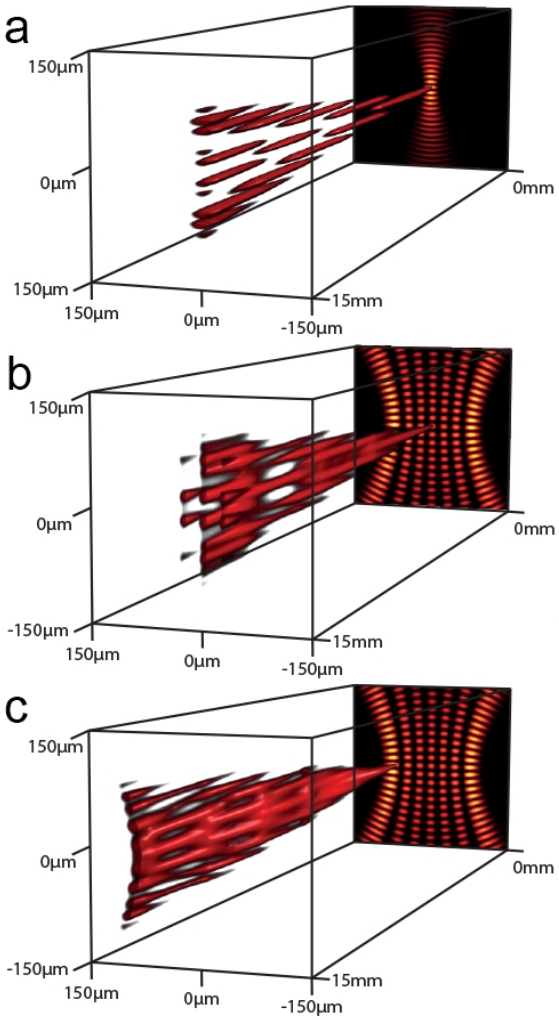

Figure 5. Gaussian probe beam propagation in Mathieu lattices: (**a**) 0th order Mathieu lattice; (**b**) 6th order Mathieu lattice, central; (**c**) 6th order Mathieu lattice, outer. Reprinted with permission from [53] © Optica Publishing Group.

Nonlinear self-action of elliptic Mathieu beams leads to the formation of high-intensity filaments, which rotated in the direction determined by the energy flow, forming chiral Mathieu photonic structures [54]. The formation of chiral Mathieu lattices is observed only in a limited regime with proper parameters for the nonlinearity and structure size (Figure 6). An investigation of chirality with other classes of beams (diffracting Laguerre–Gaussian beams) is described thoroughly in the next section.

Two-dimensional Fibonacci photonic structures are optically induced, which are supposed to be among the most ordered realizations of deterministic aperiodic patterns [18]. For their generation, nondiffracting Bessel beams are used as waveguide formation entities (Figure 7). It is constructed as an experimental system for the realization of disordered lattices by a single optical induction process in parallel using nondiffracting beams

and numerically precalculated disordered patterns with adjustable disorder degrees [55] (Figure 8).

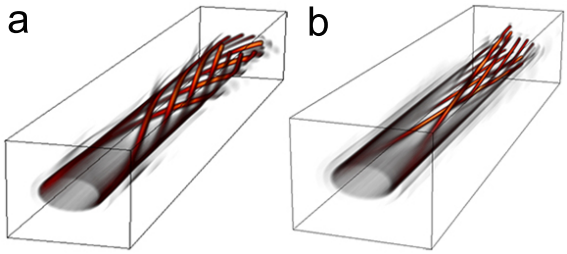

Figure 6. Chiral Mathieu photonic lattices made with Mathieu beam structure size of (**a**) 15 μm, and (**b**) 25 μm [54].

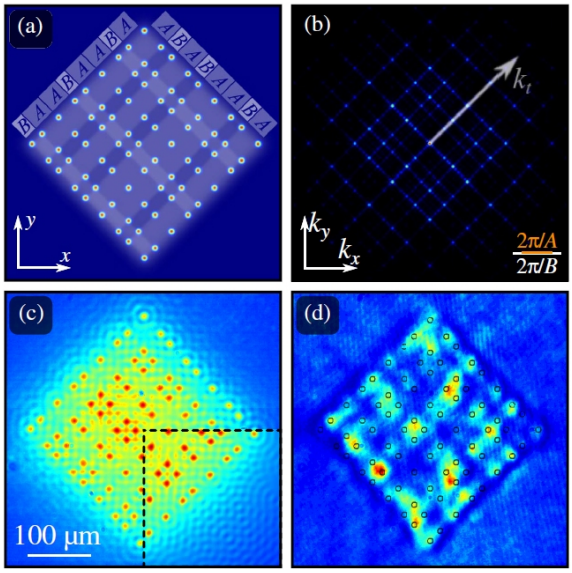

Figure 7. Optical induction of photonic lattice in photorefractive crystal SBN: Fibonacci photonic lattice generated with Bessel beams. (**a**) Fibonacci lattice with lattice spacing following Fibonacci words (indicated alongside), (**b**) spatial spectrum $S(k_x, k_y)$ according to lattice shown in (**a**), (**c**) measured effective intensity with Bessel beam lattice sites taken by multiple-shot illumination at the back face of the crystal. The bottom right quadrant shows according to numerical simulation, and (**d**) experimental output for plane-wave probing (contours indicate waveguide positions). Reprinted with permission from [18] © Optica Publishing Group.

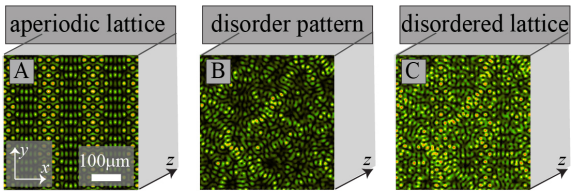

Figure 8. Optical induction of aperiodic and disordered aperiodic Mathieu photonic lattice in photorefractive crystal SBN: (**A**) aperiodic lattice, (**B**) disordered pattern, and (**C**) disordered lattice. Reprinted with permission from [55] © Optica Publishing Group.

3. Structured Light: Probing Chirality in Molecular Systems Using Diffracting Laguerre–Gaussian Beams

Although the optical properties of a material can be understood using the more-than-150-year-old Maxwell's equations, the fundamental structure–property relationship between light and matter remains very relevant. Particularly interesting are the optical properties of chiral materials (different interactions with left and right circularly polarized

light), a class of materials that is of fundamental importance in all scientific fields, especially in life sciences because all biological entities are mostly composed of chiral molecules. Chiral molecules are not superimposable on their mirror image and occur in two different forms, called enantiomers. Chiral materials have unique optical properties. For example, they have a different interaction with left- and right-hand circularly-polarized light, termed optical activity, allowing optical interrogation of each enantiomeric form. Experimental methods to study chiral materials and discriminate between enantiomers mostly rely on circular dichroism (CD), and optical rotation (OR). These optical activity effects can be explained by interferences between electric-dipole (ED) and magnetic-dipole (MD) contributions to the optical response. Electric-quadrupole (EQ) interactions can also contribute, but in isotropic systems, they average to zero and therefore EQ contributions are rarely invoked to explain CD and OR [56].

Apart from linear momentum along its trajectory, light can carry a nonzero angular momentum. When light is circularly polarized and in the paraxial regime, the photons carry a spin angular momentum (SAM) of $\sigma\hbar$ where σ can either be $+1$ (for LCP) or -1 (for RCP). Hence, optical activity effects such as CD and OR originate from the interaction of chiral materials with the SAM of light. In 1992, Allen et al. [57] showed that photons can carry an additional orbital angular momentum (OAM) apart from spin. The total angular momentum is thus the sum of a spin part depending on polarization, and an orbital part with a certain spatial distribution of the momentum vector. If we consider a plane wave, where electric field $\vec{E}$ and magnetic field $\vec{B}$ are transverse with respect to the direction of propagation, the cross-product results in the energy flux vector (Poynting vector) parallel to the direction of propagation. This means that in free space the direction of momentum flow is parallel to the direction of light propagation. To attain a helical phase front (carrying OAM), $\vec{E}$ and $\vec{B}$ are transverse to the phase fronts, but not to the propagation direction. This results in a momentum flow not only in the z direction but around the beam axis as well. Within the paraxial approximation, we can say that a photon in a helical phase front carries a momentum of $\ell\hbar$ where $\ell \in \mathbb{Z}$ is the topological charge representing the multiplicity (the number of twists within a wavelength) with the sign representing the twisting direction of the helical wavefront. If one were to look towards such a Laguerre–Gaussian (LG) beam, it would appear doughnut-shaped due to the phase singularity at the middle of the phase cross-section (Figure 9).

Up to now, Laguerre–Gaussian light has been used for various applications, and many excellent reviews are available on this topic [58,59]. However, in this paragraph, we would like to focus on the electronic interaction of Laguerre–Gaussian light with chiral matter as a new spectroscopy method. Indeed, a central question regarding their interaction with matter in the spectroscopic framework remains still unanswered. In theory, ℓ can go up to infinity but since infinitely large beam sizes do not exist, the topological charge is limited by the aperture size. The optical vortex thus propagates with a helical phase defined as $e^{i\ell\phi}$, where the gradient of the azimuthal phase results in the OAM.

A central question remains how the OAM of such a vortex beam can engage with chiral matter other than in merely exerting mechanical torque, acting as an optical spanner [60]. It seems rather intuitive that, because the spin part of angular momentum can infer optical activity in chiral materials, OAM can do it as well. However, the scientific community has been divided on the physical mechanism through which this occurs. Initial theoretical work showed that the helicity of optical vortices cannot engage with the chirality of a molecular system [61–63]. In that work, the authors considered the classical electric-dipole and magnetic-dipole interactions to the optical response, as is usually performed to describe the interaction of chiral materials with SAM. However, they did not exclude the possibility of interaction through an EQ mechanism. The first experimental investigations were initiated by Araoka et al and Löffler et al. The former investigated solutions of an enantiomerically pure helicene bisquinone derivative, the latter focused on a cholesteric polymer [64,65]. Both studies showed that OAM is not specific in its interaction with chiral matter. Only circular polarization, associated with SAM, can engage with materials chirality. However,

it was not until many years later that it was demonstrated that the OAM of light can indeed electronically interact with chiral matter [66]. They showed that light with OAM of $+l_z$ and $-l_z$ interacts differently with the enantiomers of chiral systems. The observed difference effect was dependent on the topological charge and was termed helical dichroism. The material used in these experiments was a hybrid layered material consisting of chiral organic molecules and plasmonic and superparamagnetic nanoparticles [66]. The authors showed that one needs to invoke electric-quadrupole contributions to describe the optical interaction with OAM. Later theoretical work indeed confirmed that EQ interactions are crucial in describing the interaction of OAM with chiral matter [7,67,68].

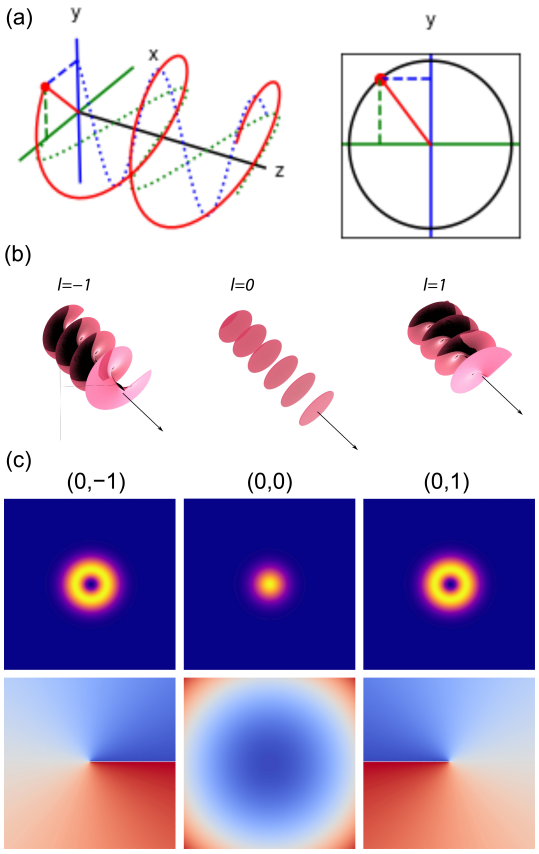

Figure 9. (**a**) Electric field propagation of circularly polarized light (in a Gaussian beam), carrying spin angular momentum. (**b**) Stylistic representation of wave-front propagation of Gaussian beam with OAM quantum number of zero and Laguerre–Gaussian beams with OAM quantum number of 1 and −1. (**c**) Two-dimensional representation of intensity and phase according to the beams represented in (**b**).

Since then, helical dichroism has been observed in other systems, but mostly in nano or microstructures—systems that are not purely molecular in nature. For example, extremely strong helical dichroism that changed with the sign and magnitude of the topological charge was observed by Ni et al. in two-dimensional chiral nanostructures [69]. The same authors observed very strong vortical differential scattering, i.e., a different scattering efficiency for opposite topological charges, in chiral (helical) microstructures and showed that the chiro-optical response can be carefully tuned by the geometry of the structures [70,71]. Indeed, by matching the structural dimensions with the dimensions of the vortex beam, they were able to optimize the vortical differential scattering geometry. Furthermore, adsorbing chiral molecules (L-and D-phenylalanine) on the microstructures allowed them to discriminate between the enantiomers. Recently, it was demonstrated that helical dichroism can even be observed in purely molecular systems by exploiting nonlinear optical processes such as multi-photon absorption. Isotropic chiral solutions of simple organic molecules were

shown to exhibit helicity-dependent nonlinear absorption [72]. The authors also stressed the importance of quadrupole contributions that occur due to laser-induced orientational effects in the solution.

From the above, it is clear that the study of the interaction of vortex beams with chiral matter is still in its infancy. However, recent experiments have shown that chiro-optical techniques based on OAM can be an extremely valuable addition to the portfolio of currently available chiro-optical spectroscopies. One of the main advantages of OAM is that the momentum values are not limited to $\pm\hbar$ as is the case for SAM but can in principle take on any integer value. This yields an additional degree of freedom to explore the interesting properties of chiral molecules. Furthermore, chiro-optical techniques based on OAM need not to be limited to linear optical processes such as absorption, transmission, or scattering. Multi-photon techniques such as two-photon absorption, two-photon fluorescence, or second-harmonic generation may in fact be much more sensitive to probe helical dichroism.

4. Structured Light: Holographic Applications

Since Gabor's first hologram [73], the holographic technique has largely grown and is widely used in different fields, such as security [74], data storage [75], cultural heritage [76], as well as imaging and medicine [77]. Basically, holography is an interferometric technique: an interference pattern (i.e., the hologram) is generated by superimposing two coherent beams, named the object and reference beam. The hologram can be recorded on a photo-sensitive medium or, in the case of digital holography (DH), on a CCD. The original object wavefront can be obtained by illuminating the hologram with the only reference beam; in DH, this operation is numerically performed to retrieve the whole complex object beam.

Holography has been used to generate and detect structured light beams [78]. However, this section aims to report on how structured light can improve the performance of holographic techniques. Therefore, with this goal in mind, the following aspects will be examined: phase shifting and resolution enhancement, memory and high-security encryption, 3D communications, and nonlinear and quantum holography.

In in-line DH, where the object and reference waves are overlapped, the reconstruction of the object image is difficult due to real and virtual images overlapping. In order to overcome this drawback, an off-axis configuration or phase-shifting approach can be implemented [79]. However, a high-quality off-axis hologram is difficult to record due to the limited bandwidth of the off-axis system which is feckless with respect to the space-bandwidth product of the optical image amplitude [80]. Phase-shifting DH allows for reconstruction of high-resolution images making full use of the bandwidth of the optical detector; however, it generally requires multi-exposure holographic recording while shifting the phase of reference field by an integer fraction of 2π [81]. In 2004, the use of an optical vortex (OV) beam as the reference wave for phase-shifting holographic recording was proposed [82]. The required phase shifts were obtained by generating four different angled optical vortices; this optical vortex phase-shifting holography could offer a new perspective in research on the dynamics of the OV in linear or nonlinear materials.

For high-throughput dynamic imaging, single-shot phase-shifting DH is highly desirable. In this context, illumination with structured light could offer a new approach. Zhang et al. proposed to use an OV beam with different eccentricity and topological charge as the reference beam into a modified Michelson interferometer with two different 4f-telescopes [83]. A cosine grating is positioned in the object path allowing to produce at once two-copy images of the measured object beam in the other beam path, leading to their interference with the vortex reference wave in one single exposure (see Figure 10a). Parts of the reference beam can be used to remove zero-order terms in the reconstruction process. The reported experimental results are in good agreement with the theoretical analysis. The same authors reported a Mach-Zehnder interferometer with a vortex beam (amplitude-only Fermat-spiral sieve) as the reference signal and a splitting grating in the object arm [84] which splits the object wave into four parts positioned in the four quadrants of the vor-

tex reference wave. This scheme, shown in Figure 10b, gives rise to a single-exposure interference pattern that contains the four frames of phase-shifting holography.

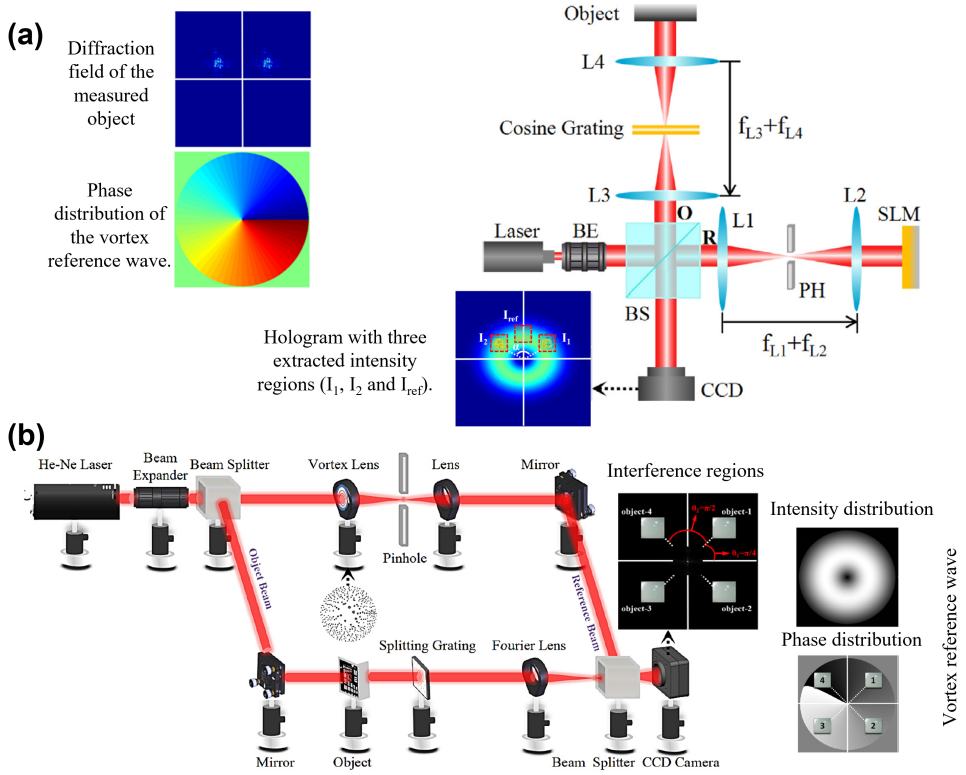

Figure 10. Phase-shifting digital holography set-ups with vortex beam in one single exposure. (**a**) Two interference patterns. Laser: He-Ne laser; BE: beam expander; BS: beam splitter; O: object wave; R: reference wave; L1-L4: condenser lens; PH: pinhole. Reprinted from [83] with permission from Elsevier. (**b**) Four interference patterns [84]. ©Astro Ltd. Reproduced by permission of IOP Publishing Ltd. All rights reserved.

By combining DH with optical microscopy, digital holographic microscopy (DHM) can be implemented to image semi-transparent and transparent objects. Generally, DHM spatial resolution is limited by the wavelength (λ) and the numerical aperture (NA) of the imaging system [85]. In order to improve the resolution of intensity images, structured illumination microscopy (SIM) has shown high potential [86]. Since 2010, when super-resolution in holograph was demonstrated using structured illumination [87], this research field has attracted increasing interest. In 2013, Gao and co-workers reported an improvement of the resolution thanks to the use of structured light generated by a spatial light modulator (SLM) which illuminates the object projecting fringes with different orientations and phase shifts without mechanical motion [88]. Autofocusing has been also achieved for both amplitude and phase objects by detecting the minimal difference between the reconstructed images related to different diffraction orders of the structured illuminations. Alternatively, fringe patterns can be generated by a digital micromirror device (DMD) and, when applied as illumination of the object in DHM, 3D refractive index tomographic images of samples have been retrieved [89].

Structured illumination generated by a sequence of differently oriented sinusoidal gratings onto an SLM has been directed to a Mirau microscope objective in DHM, forming its image on the sample and leading to a resolution enhancement of 35% with respect to standard DHM [90]. One-dimensional gratings with different orientations can be replaced by single 2D gratings, allowing increased resolution in multiple directions. Moreover, deep learning has been recently proposed to further enhance the reconstruction efficiency and the accuracy of DHM imaging based on structured illumination [91].

Among its different applications, holography is considered a crucial platform for optical encryption and data storage. Despite the possibility of holograms reaching nanometre-scale resolution thanks to recent progress in metasurface technologies, the hologram bandwidth is still too low for practical applications. This drawback has been recently addressed by storing information in the orbital angular momentum (OAM) of light: basically, the incident OAM beam is the key to unlocking the specific information. Multi-bit OAM-multiplexing holograms can be obtained by high-order OAM beams allowing an all-optical holographic encryption with a high level of security. The basic principle of OAM holography is reported in Figure 11. Starting from 2019, Fang and colleagues firstly demonstrated a multiplex information of four channels based on a meta-hologram consisting of GaN nanopillars with discrete spatial frequency distribution (see Figure 11a) [92]. Then, in 2020, they reported an OAM holography technology able to multiplex up to 200 independent OAM channels and realized by a polymer-based metasurface [93]. Finally, the same research group reached an ultra-high-capacity holographic information system able to have up to 2^{10} OAM-specific holographic images [94]. This goal has been achieved by engineering a sampling array period in order to match the spatial-frequency distribution of a precise incident OAM beam. The design approach of the 10-bit OAM-encoded hologram as well as the OAM code chart are shown in Figure 11b,c.

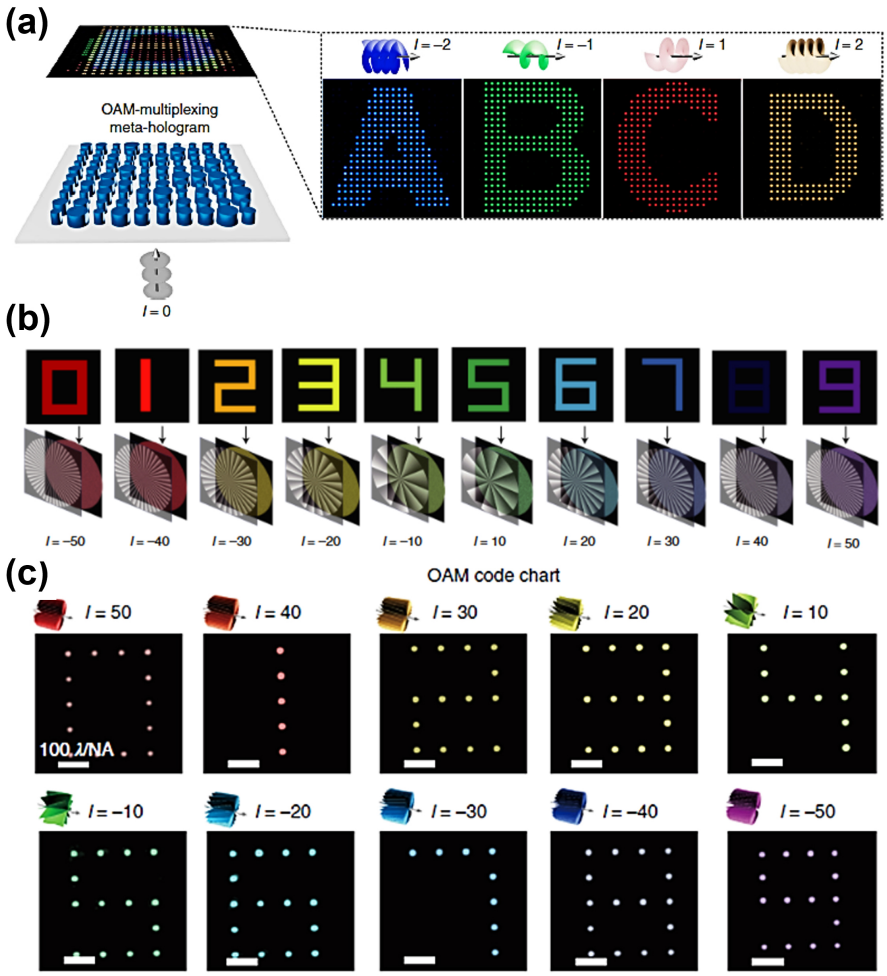

Figure 11. (**a**) Schematic of an OAM-multiplexing meta-hologram: multiple OAM-dependent holographic images can be reconstructed [92]; (**b**) design approach for a 10-bit OAM-multiplexing hologram for high-security holographic encryption [94] , reproduced with permission from SNCSC; (**c**) OAM code chart: 10 high-order OAM modes are used to reconstruct the 10 OAM-dependent digits based on the OAM-multiplexing hologram [94], reproduced with permission from SNCSC.

High-security holographic encryption has been also obtained by using an all-dielectric birefringent metasurface for holographic encryption: the OAM selective holographic information can be retrieved only if the incident beam has the right topological charge and polarization state [95].

The holographic technique has been traditionally applied in the linear optical regime; however, in the recent past, the concept of nonlinear holography has been introduced to shape the wavefront of the light emitted by nonlinear optical process [96]. In this context, the use of OAM multiplexing nonlinear holography has been experimentally demonstrated to overcome the crucial restriction of wave coupling in nonlinear optical process [97]. This approach, demonstrated in a type-II second harmonic generation (SHG) process, allows wavelength-multiplexing nonlinear holography (WMNH) and can be also enhanced by encoding multiple patterns for each wavelength leading to an increase in information channels, thus proving for the first time the multichannel nonlinear holography (MCNH). The basic principles of both WMNH and MCNH applied in type-II SHG are reported in Figure 12.

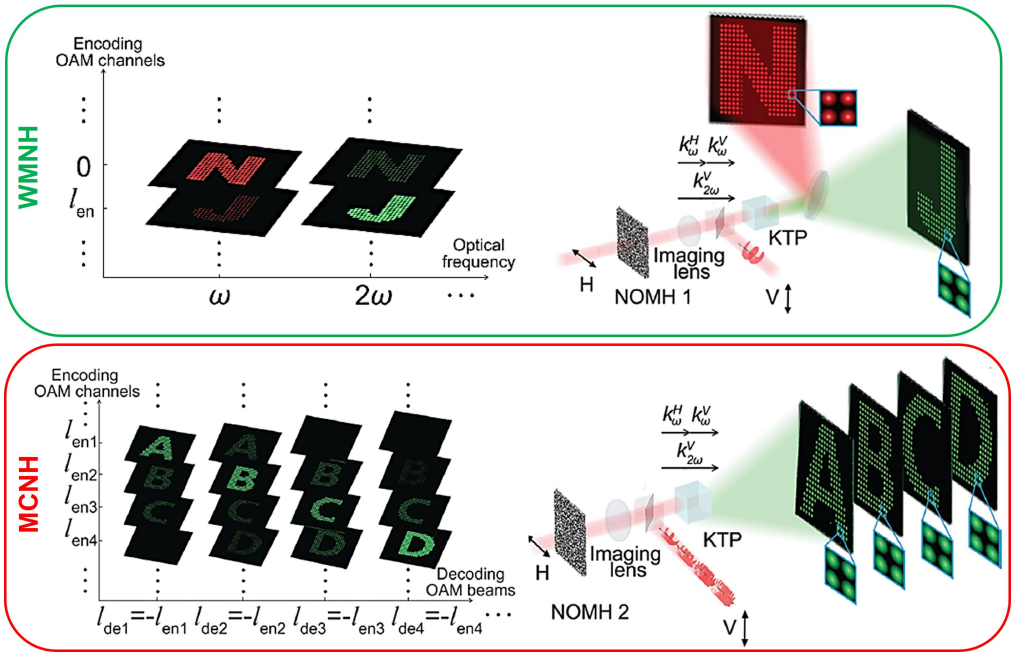

Figure 12. Concepts of WMNH (up) and MCNH (down). NOMH: nonlinear OAM-multiplexing hologram; KTP: nonlinear material ($KTiOPO_4$). In the SHG process there are two incident fundamental beams (k_ω^H and k_ω^V, H and V are the horizontal and vertical polarizations, respectively) and the output is the second-harmonic beam ($k_{2\omega}^V$, vertically polarized). WMNH in a type-II SHG process allows to separately reconstruct letters N and J in forward wave and SHG wave, respectively; MCNH in a type-II SHG process permits to reconstruct letters A, B, C, and D in SHG wave [97].

Taking advantage of quantum interference in a nonlinear interferometer between correlated signal and idler photon pairs generated by spontaneous parametric downconversion (SPDC), Töpfer et al. overcame the limited detection for wavelengths outside the visible range [**?**]. In detail, they designed a phase-shifting holography with nonclassical states of light and demonstrated that both the amplitude and phase of the photons transmitted/reflected from the object can be reconstructed, hence obtaining an image of the object even if the same photons are never detected. With such a configuration, the reference for holography corresponds to one of the photons of the pair.

Another interesting and widely used application of the holography technique is 3D imaging and display technologies, useful for 3D communication. On this line of arguments, a potential solution to telepresence in the metaverse has been proposed by developing a real-time 3D system integrating the detection, hologram generation, transmission, and

visualization [99]. This system is based on a structured light camera (slower, with a higher resolution and depth accuracy with respect to a CCD) and a light field camera (with a high frame rate) that acquired the 3D scene; then, phase-only holograms are computer-generated by an algorithm based on rendered depth images and shading images (layer-based angular spectrum method), as sketched in Figure 13a. A 4K SLM is used to dynamically reconstruct the phase-only holograms. A 3D model of a human body has been captured and rendered into videos by rotating 360° around the central axis (see Figure 13b), showing the abilities of this system for 3D communication in the near future.

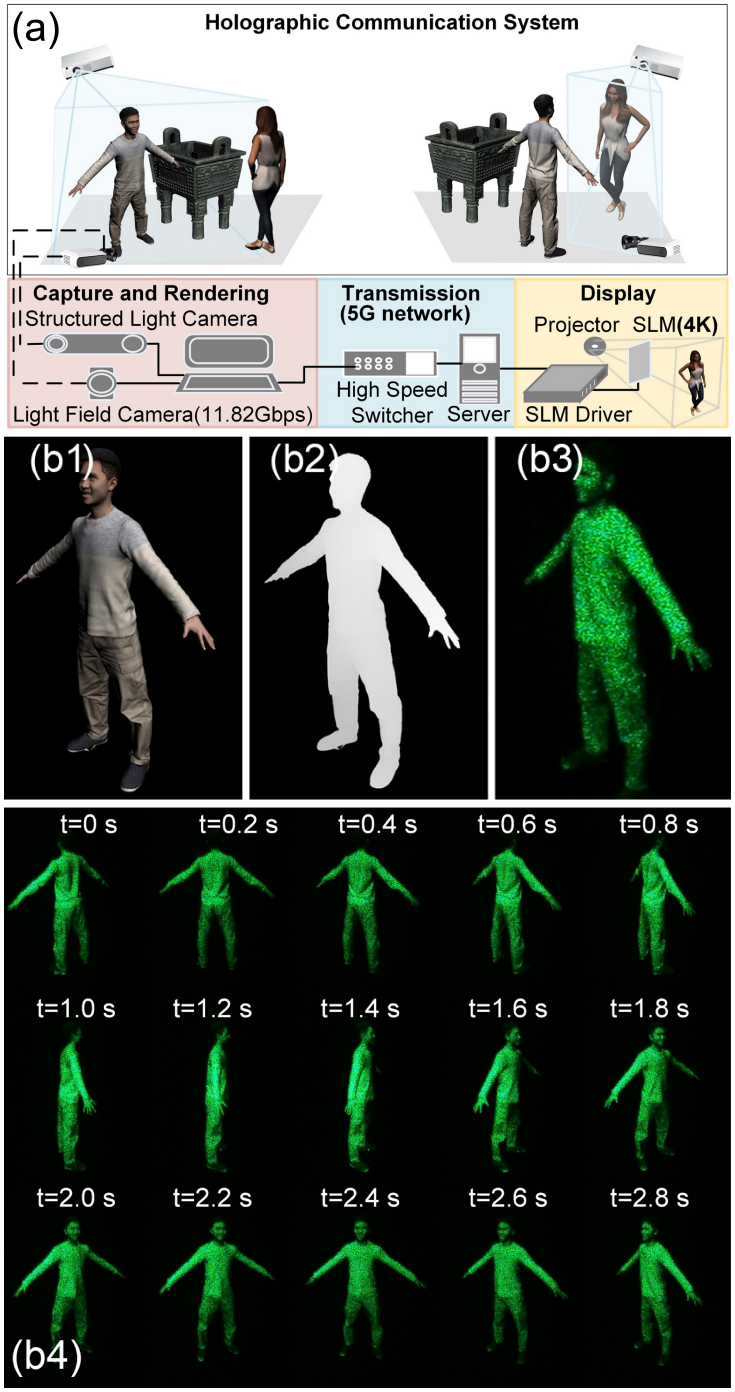

Figure 13. (**a**) Holographic communication system; (**b**) experimental results: (**b1**) color maps of target objects, (**b2**) depth maps of target objects, (**b3**) reconstructions of the objects, (**b4**) dynamic holographic 3D display. Reprinted from [99] with permission from Elsevier.

The significant research efforts, partly reported in this section, highlight that in the last few years structured light beams have become an important tool for holography technique to strongly enhance its performance, open up new perspectives, and pave the way for a wide range of its potential applications.

5. Structured Light: Quantum Viewpoint and Applications

Many of the remarkable properties of structured light beams originate from classical electromagnetism, a world fundamentally ruled by Maxwell's equations and wave physics. However, when the light intensity reaches extremely low values, the beams exhibit discrete behaviors that conform to the quantized rules of optics and light–matter interactions. In quantum optics, photons become the building blocks of structured beams. In a simple picture, photons carry not only a discrete quantum of energy but linear and angular momentum as well. The classical beam qualities emerge thus from the individual properties of photons, with classical interferences arising from quantum superpositions. Nevertheless, to describe the beam granularity, especially when correlations are involved, we must refer to the quantum formalism. Indeed, the main conservation laws of physics affecting classical optics, including phase matching in nonlinear optics, may produce entanglement in energy, momentum, and angular momentum at the quantum level. Entanglement is associated to nonseparable quantum states of composite systems. Multi-photon entanglement enables the fundamental testing of nonlocality in quantum mechanics through the violation of Bell inequalities. Interestingly, many structured light beams already exhibit nonseparable, local correlations of their degrees of freedom in the classical description of the beam [100,101]. Structured light concepts often overlap the quantum–classical boundary. This section briefly reviews the properties of structured light beams from a quantum perspective, highlighting the usefulness of structured light beams for fundamental quantum studies, as well as a few applications relevant to quantum technologies.

Without considering the temporal structure of the wavepacket, the quantum state of a photon from a paraxial beam propagating along the z axis can typically be written as

$$\sum_{i=0}^{\infty}\sum_{j=0}^{\infty}\left(c_H^{ij}|H\rangle\otimes\left|\mathcal{M}_{ij}\right\rangle+c_V^{ij}|V\rangle\otimes\left|\mathcal{M}_{ij}\right\rangle\right)e^{ik_z z}. \tag{2}$$

The kets $|H\rangle$ and $|V\rangle$ form the basis of the polarization degree of freedom (here, the horizontal and vertical polarization states). The indices i and j label the various orthogonal transverse modes $\left|\mathcal{M}_{ij}(\vec{r}_\perp,z)\right\rangle$, since the spatial mode structure is conserved at the single-photon level. The pair of indices arises from different mode families, which depend, in particular, on the associated coordinate system (among them, the Hermite–Gauss modes in Cartesian coordinates, the Laguerre–Gauss modes in cylindrical coordinates, or the Mathieu–Gauss modes in elliptic cylindrical coordinates, for example). The complex amplitudes c_H^{ij} and c_V^{ij} weigh the contributions of the different polarization and spatial modes to the quantum state, as well as set their relative phases. Often, one will work with a reduced set of modes, so that only a few coefficients may contribute to the structured light beam, if not a single one. When the coefficients are factorizable, i.e., if we can write $c_H^{ij}=m_{ij}C_H$ and $c_V^{ij}=m_{ij}C_V$, the polarization and the spatial structures of the light are decoupled. In that case, the state is separable: it can be expressed as a single tensor product

$$(c_H|H\rangle+c_V|V\rangle)\otimes\sum_{i=0}^{\infty}\sum_{j=0}^{\infty}m_{ij}\left|\mathcal{M}_{ij}\right\rangle e^{ik_z z}. \tag{3}$$

Otherwise, the polarization and the spatial degrees of freedom are correlated, with a quantum state (2) appearing formally as entangled, even though a single photon is involved.

One of the significant benefits of structured light beams as quantum resources is their ability to carry orbital angular momentum (OAM). The spin angular momentum (SAM) of light, i.e., its polarization, corresponds to a two-level quantum system, known as a

quantum bit, or qubit. Polarization qubits are widely used in quantum optical studies. Geometrically, their pure states correspond to the full surface of a sphere (Figure 14), called the Bloch sphere in the context of quantum physics, or the Poincaré sphere in the context of classical polarization optics [102] (actually, a representation of $\mathbb{C}\mathrm{P}^1$, the complex projective line [103]). Left and right circularly polarized photons carry $S_z = \pm 1\hbar$ of angular momentum. However, OAM states are associated to integer quanta $L_z = \ell\hbar$ of orbital angular momentum. OAM orthogonal modes can thus build higher-dimensional quantum spaces, defining qudits. OAM qudits benefit experimentally from the light's advantage of interacting very little with its environment, avoiding decoherence, and thus preserving quantum superpositions and entanglement over long distances. Unfortunately, the complicated geometry of the qudit state space prevents a simple generalization of the Bloch sphere representation [103], even in the three-dimensional, qutrit case [104]. Nevertheless, transpositions of the polarization Poincaré sphere describe two-dimensional subspaces of OAM modes [105] (Figure 14), as well as higher-order Poincaré spheres depict the polarization structure of vortex beams in terms of the total angular momentum [106], along with their associated Pancharatnam-Berry geometric phase acquired under parametric evolution on this sphere [107]. For example, structured light can acquire a geometric phase when propagating in helical fibers [108]. Representations of generalized Hermite–Laguerre–Gauss modes exist now in terms of Jones vectors [109], rays [110], and the Majorana stellar representation of the modes [111]. A synthetic approach in terms of SU(2) coherent states [112] englobes these prior descriptions [113]. We note in passing that the so-called fractional angular momentum vortex beam actually consists of a quantum superposition of many integer OAM states [114,115], generating high-dimensional spatial entanglement in twin photons [116].

High angular momentum states are advantageous for quantum communications, including quantum key distribution [117] (commonly referred to as QKD) because qudits carry more information than qubits and are theoretically more secure (for example, they are harder to clone optimally [118]). Atmospheric turbulence generally degrades the beam spatial profile in practice [119], including for vector beams [120] (although they confer an enhancement [121]). Nevertheless, it is possible to avoid the consequences of distortions, notably by using structured states invariant under turbulence [122] (the latter are not based on OAM, though), or to improve pattern recognition at detection by exploiting machine learning [123]. Entanglement is a key concept in many quantum information processing tasks. Early on, it was realized that spontaneous parametric down-conversion (SPDC) in nonlinear crystals, with a Gaussian pump, produced pairs of photons entangled in OAM (each photon carrying opposite values, considering a pump photon with no OAM) [124]. More explicitly, the conservation of angular momentum can yield entangled states of the modes of twin photons, such as

$$|\psi_{AB}\rangle = c_{\ell,-\ell}|\ell\rangle \otimes |\ell_p - \ell\rangle + c_{-\ell,\ell}|\ell_p - \ell\rangle \otimes |\ell\rangle, \tag{4}$$

for a pump photon of angular momentum ℓ_p, assuming that only two modes are produced, of angular momentum $\ell\hbar$ and $(\ell_p - \ell)\hbar$. Here, the tensor product involves the states of different photons, meaning correlations can become nonlocal, contrary to the single-photon correlations described by Equation (2). SPDC involving structured light [125–127] is thus at the heart of many sources of photon pairs entangled in OAM. Interestingly, spin to OAM coupling may occur in nonlinear conversion processes [128], going beyond the simple phenomenon illustrated by (4). For the interested reader, a recent review [129] brings into focus the specificity of nonlinear optics with structured light propagating in bulk crystals. SPDC provides heralded single photons as well, that can be tailored to specified beam shapes using standard structured light technologies (such as spatial light modulators and holographic plates): for example, Airy single photons put in shape after SPDC [130] (actually, the entanglement resulting from SPDC can even produce correlated Airy photons [131] or correlated Airy-non-Airy photons [132]). This technology enabled the creation of entangled photon pairs in high dimensions and confirmed their entanglement through

the measurement of a Bell inequality violation. For example, structured beams of entangled photons demonstrated quantum cryptography with qutrits [133], as well as quantum key distribution implemented in a 7-dimensional basis [134] or using mutually unbiased bases encoded in OAM [135]. Over the years, structured light technology has substantially pushed the boundaries of achievable entanglement: notably, by entangling high quantum numbers of OAM [136,137]; by using hybrid entanglement schemes involving several degrees of freedom of photons, such as coupling spin and orbital angular momentum in single photons [138] or in entangled photon pairs [139]; by entangling more than two degrees of freedom [140], such as mixing polarization, OAM, and time-frequency modes [141], degree of polarization [142,143], paths [144], or wavelength [145]; by increasing the number of photons entangled in OAM [146,147] (the last example involves six photonic qutrits); and by increasing the amount of entanglement using high-dimensional spaces, for example involving many spatial (Laguerre–Gauss) modes of entangled photons [148]. For a review of hyper-entanglement schemes (involving N photons entangled in $d-$dimensional qudits), we suggest [149]. Recently, the spatial dependence of both classical and quantum manifestations of entanglement were resolved in photon and biphoton vector modes [150,151], indicating that entanglement must not necessarily be a global property. Storing and converting OAM information is also crucial for quantum communication purposes. Memories were notably realized using electromagnetically induced transparency in cold atomic ensembles (for a recent long-lived qutrit memory [152]), with doped crystals [153], or with paths [154]. In order to develop technologies for quantum key distribution networks, entanglement was successfully transferred from free-space OAM modes to energy-time entanglement in fibres [155], and OAM transmission in fibres was demonstrated [156]. Entangled photons of structured beams may also be useful for quantum metrology and imaging, for example in generalizations of quantum ghost imaging techniques [157] or for sparse sensing [158].

OAM impacts light beam interactions with matter at the quantum level, as total angular momentum exchanges occur in integer values of $\hbar$. However, total angular momentum conservation in these interactions does not preserve a priori SAM and OAM individually, affecting selection rules in spectroscopy [159]. Even in a Gaussian beam, photons may contribute OAM to complete a transition [160], since orbital angular momentum can be defined with respect to an arbitrary off-axis origin. Transfers of photon OAM to matter were observed for bound electrons in trapped ions [161] and evaluated theoretically for atoms [162], while light vortices might produce rare superkicks to atoms [163,164]. Interactions of structured light with matter can leave the matter in a desired quantum state, making it useful for applications, such as acting as an entangling gate for two atomic qubits [165], or generating vortices in quantum matter (for example, imprinting the OAM on the spin texture in semiconductors [166], producing coherent atomic vortices in Bose-Einstein condensates [167,168], or storing OAM information from ultra-short pulses in the rotational coherences of molecules in the gas phase [169]). Structured light beams affect the selection rules of atomic transitions in a position-dependent way [170]. Conversely, light–matter interactions may probe the OAM structure, for example through atomic photoionization [171]. The interplay between chirality, optical activity, and OAM is discussed in more detail in Section 3 of this paper. Subtly, a quantum study of the atomic emission [172] and absorption [173] processes in the close vicinity of the vortex of an OAM-carrying beam enables probing how the classical phase singularity becomes blurred at the quantum level, due to the quantum uncertainty and the quantum vacuum. In particular, absorption near the vortex line defines a quantum core where absorption produces predominantly a spinning motion of the atom around its center of mass, contrary to absorption occurring in the coherent, classical field far from the vortex [173], which causes negligible spinning of the atom. Let us note in passing that the rotations of atoms, molecules, and small objects that are induced by the classical mechanical torque associated to OAM beams are of considerable interest, including for studying quantum effects. Structured light beams can act as optical spanners, where the beam total angular momentum, combining both SAM and OAM, contributes to the induced rotational motion of the particle [174,175]. For a particle

located off-axis, the different mechanical actions of SAM and OAM transfer can be tracked experimentally, as SAM induces spinning of the particle around its own axis, while OAM transfer makes it rotate around the beam axis [176–179]. The mechanical motion of atoms in structured light was extensively reviewed [180]. Structured light enables optical trapping and microparticle manipulation [181–183] (there is a nice earlier account of field [184] in addition to the recent reviews [182,183]). The in-depth study of particle rotations promises many quantum applications [185], such as probing the collapse of macroscopic quantum superpositions by tracking orientational quantum revivals in nanorotors [186], or evidencing quantum friction [187] and rotation-induced quantum phases [188]. Mechanical rotations probe the complex structure of vortex beams as well, such as in this study of beams evidencing transverse (instead of longitudinal) phase singularities and transverse OAM [189]. To conclude this part on structured-light–matter interactions, let us add that new material developments are crucial to efficiently tailor the structured light properties at the single-photon level, notably through the use of metasurfaces [190–192].

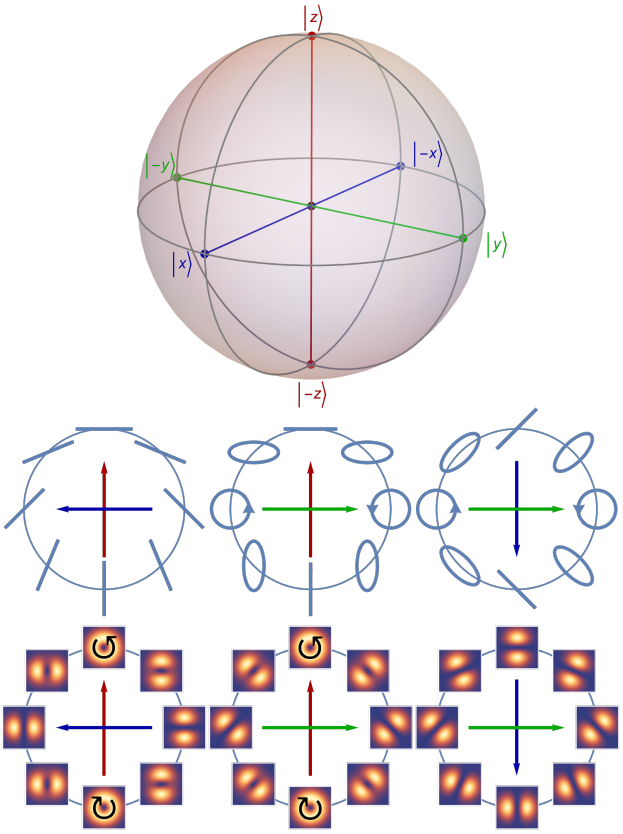

Figure 14. Top: Bloch sphere representation of a two-level quantum system. Any pure quantum state can be represented as a coherent superposition $\cos(\theta/2)|z\rangle + \sin(\theta/2)e^{i\varphi}|-z\rangle$ of the two basis states $|\pm z\rangle$, with θ and ϕ corresponding the usual spherical coordinates of points on the unit sphere. Mixed states correspond to points inside the sphere. They can be described with density operators as $\hat{\rho} = (1+p)/2|\theta,\phi\rangle\langle\theta,\phi| + (1-p)/2|\pi-\theta,-\phi\rangle\langle\pi-\theta,-\phi|$ with $p \in [0,1]$ linked to the state purity. First row: Polarization ellipses for a polarization qubit with $|z\rangle = |H\rangle$ (horizontal), $|-z\rangle = |V\rangle$ (vertical), $|x\rangle = |D\rangle$ (diagonal), $|-x\rangle = |A\rangle$ (anti-diagonal), $|y\rangle = |R\rangle$ (circular right), $|-y\rangle = |L\rangle$ (circular left), along the zx, zy, and xy great circles, respectively. The red arrow indicates the z axis, the green arrow, the y axis, and the blue arrow, the x axis. Second row: Intensity profiles of beams generated by the coherent superpositions of the Laguerre–Gauss beams $LG_0^{\pm 1}$ with $|z\rangle$ representing the LG_0^1 mode and $|-z\rangle$ representing the LG_0^{-1} mode, also along the zx, zy, and xy great circles, respectively. We can observe that the superposition generate the Hermite–Gauss modes HG_{10} for $|x\rangle$ and HG_{01} for $|-x\rangle$. Equivalent representations also exist for two-level systems based on coupled degrees of freedom (for example with $|z\rangle = |R\rangle \otimes \left|LG_0^{-1}\right\rangle$ and $|-z\rangle = |L\rangle \otimes \left|LG_0^{+1}\right\rangle$).

At low intensities, structured light beams exhibit photon shot noise that can be detrimental to highly sensitive applications. With reduced quantum noise, sources of squeezed structured light [193,194] can improve detection, imaging, and laser position measurements (Figure 15). Thus, a quantized theoretical description of the fields and their observables is necessary to describe the various quantum statistics, for polarization [195] and vortex modes [196,197], including for phase [198], intensity, position, and angular measurements. It can be obtained from the raising and lowering operators of quantum harmonic oscillators associated to the classical electromagnetic modes, typically in the paraxial approximation, but considering the photon wavefunction [199] is also fruitful to provide the appropriate photon quantum numbers [200] and Stokes parameters [201]. An approach emphasizing symmetry at the photon level sheds light on the essential features of the quantized field operators and their associated quantum uncertainties relevant for light–matter interactions [197]. Additionally, the raising and lowering operators for OAM can be constructed from Schwinger's representation of angular momentum using pseudo-oscillators [110]. The algebraic formalism of the quantum raising and lowering operators can notably relate the mode families of purely classical paraxial beams [202], such as Hermite–Gauss or Laguerre–Gauss modes. Certain complex beams can even be described at the theoretical level with quasiparticles, such as skyrmions and hopfions [203,204], as well as effective bosonic particles [205]. One practical question is whether structured light beams preserve their useful classical properties down to the photon level. This has been shown, for example, for the self-healing properties of heralded single photons of Airy [206] (Figure 16) and Bessel [207] beams, and for the healing of entanglement in entangled Bessel beams [208]. OAM-entangled Airy biphotons were shown theoretically to be more resilient against underwater turbulences than Laguerre–Gauss beams [209]. Perhaps counter-intuitively, the photon group velocity is slower than c for a beam propagating in free space [210,211]: a simplified argument links this to the projection, on the beam axis, of the twisting movement in a beam carrying OAM, which reduces the average propagation along the axis. This effect was described in a quantum formalism using a Dirac-like equation, in which the photon acquires an effective mass [212] and in terms of bosonic quasiparticles [205]. Thus, the advent of structured light forces us to reconsider the nature of photons beyond the simple plane wave or standing wave models. Conversely, the nonseparability of many properties of photons in classical, structured light beams, as illustrated in (2), makes us revisit the notion of entanglement in a classical context [213], such as nonseparability of polarization and position or of ray-wave duality [214]. Nonseparability of classical space-time wave packets, such as in the flying doughnut, has also been studied using the tools of quantum information theory, such as fidelity, entanglement of formation, and concurrence [215], while a quantum formulation of space-time wave packets has also been developed [196]. Another point of interest for the statistical quantum description is the study of phase singularities in the global biphoton states, that manifest themselves in the detection coincidences, i.e., in the quantum correlations [216].

We wish to highlight the importance of structured light beams for fundamental studies of quantum mechanics. As an alternative to polarization qubits, OAM modes allow us to investigate higher-dimensional quantum spaces with the advantages of low decoherence. Many archetypal quantum experiments were carried out with OAM, such as Young's two-slit experiment [217,218], the verification of Heisenberg's uncertainty relations for angular position and OAM [219] (recently performed with entangled photons to test Popper's conjecture [220]), the demonstration of a delayed choice quantum eraser based on OAM and SAM [221], the realization of entanglement swapping and/or teleportation [222,223], including the teleportation multiple degrees of freedom [224] (operations that are also very relevant for quantum information processing tasks useful for quantum technologies), and performing Hong-Ou-Mandel interferences [225] to produce high-dimensional entanglement. The azimuthal phase of vortex beams affects the Wigner phase time in quantum tunnelling, effectively controlling the Hartman effect [226]. OAM modes enable the testing of local realism through the violation of Bell [227] or Leggett [228] inequalities, including

for high-dimensional systems [229] and for local degrees of freedom [230], but also of contextuality [231,232]. In addition, a nonlocal game exploiting quantum correlations to win with certainty [233], quantum correlations in optical-angle-OAM [234], and quantum steering in a set-up closing the detection loophole using hybrid OAM-polarization entanglement [235] have all been demonstrated. Bell-like inequalities for continuous variables expressed in terms of Wigner functions were violated for Laguerre–Gauss beams [236] and studied theoretically for Ince-Gauss beams [237] (which include Hermite-Gauss and Laguerre–Gauss modes as limits of their ellipticity parameter). Experimental tests of quantum mechanics and quantum technologies require generating specific quantum states such as Dicke [238], GHZ-like [213] and GHZ (entangled qutrits actually) [239] states, as well as W states. Processing these states necessitates implementing mutually unbiased bases (MUB) [135] and Bell basis [240,241], as well as building sets of quantum gates for single-photon OAM states [242–244] and two-qubit SWAP gates [245]. For additional information on the quantum aspects of structured light in high dimensions, we refer the reader to a recent tutorial [246]. Light beams carrying OAM demonstrated quantum sensing of three-dimensional rotations with parameter estimation near the optimal Cramer-Rao bound [247]. In addition, structured light beam concepts inspire applications in other fields, such as atom optics with Bose-Einstein condensates [248].

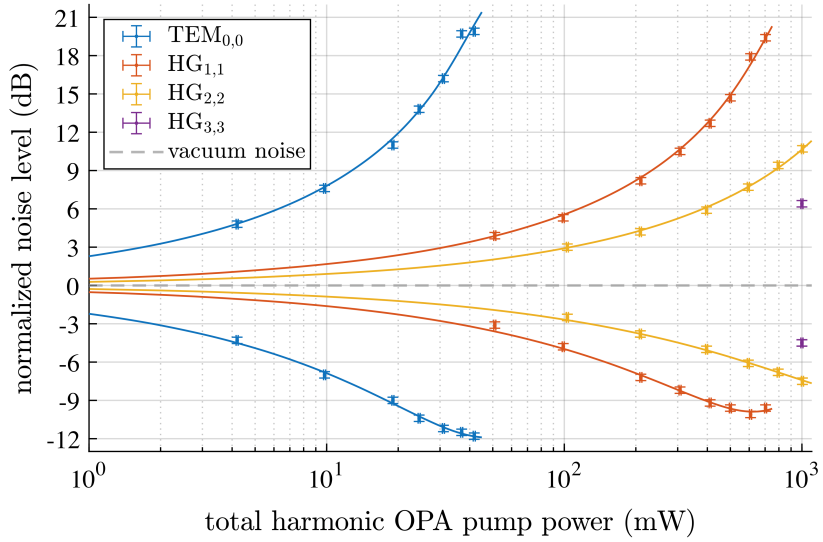

Figure 15. Noise reduction and amplification obtained for squeezed and anti-squeezed structured light, respectively (the solid line corresponds to the theoretical model). The noise reduction reaches up to 10 db for the Hermite-Gauss modes. Using higher-order spatial modes could mitigate the effect of thermal noise in advanced interferometers. Reproduced from APS under CC4.0 license [194].

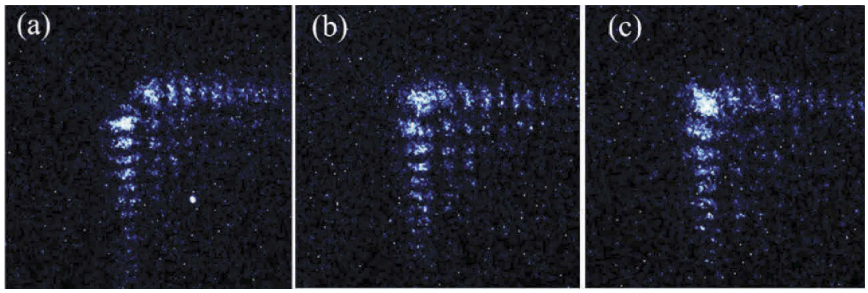

Figure 16. Self-healing of Airy photons with the main lobe blocked (the lobe is located in the top-left corner of the beam). (**a**) Intensity profile in the plane $z = 0$, (**b**) $z = 5$ mm, (**c**) $z = 10$ mm. The main lobe reappears upon the beam propagation, evidencing self-healing at the photon level. The images correspond to the accumulation of 3500 heralded single photons. Reprinted with permission from [206] © Optica Publishing Group.

A salient feature of light beams is their practical connection to quantum weak measurements, at the very boundary between classical and quantum optics. Weak measurements were introduced in 1988 by Y. Aharonov et al. to study foundational issues in quantum mechanics [249]. Since then, however, weak measurements found their way into many applications, especially because they enabled the detection of tiny physical phenomena, through what is called weak value amplification [250]. A typical weak measurement of a quantum system involves three successive steps: a pre-selection, which corresponds to setting the initial state $|\psi_i\rangle$ of the probed system; a weak unitary interaction involving the property of interest, that entangles slightly the probed quantum system with an ancilla system (also called the pointer) that will act as a quantum measuring device; and the measurement of the ancilla's final state conditioned on the successful post-selection of the system on a predefined final state $|\phi_f\rangle$ (this can be accomplished by performing a projective measurement on the system, followed by a filtering of the results of the system-ancilla joint measurement). A classic weak measurement set-up involves the light's polarization as the probed system and the transverse position of the beam center as a pointer [249] (see Figure 17). Let us note as an illustration that a usual quantum measurement of the OAM of a structured light beam involves post-selection, performed by combining a specific OAM-to-Gaussian mode converter followed by a Gaussian single-mode fibre [251]. Interestingly, the results of a weak measurement of an observable $\hat{A}$ depend on the real and imaginary parts of a complex number called the weak value

$$\langle A \rangle_w = \frac{\left\langle \phi_f | \hat{A} | \psi_i \right\rangle}{\left\langle \phi_f | \psi_i \right\rangle}, \tag{5}$$

an expression that bears some resemblance to a generalized conditional quantum average. Weak measurements are well-suited to probe fundamental issues of quantum mechanics because, as the coupling becomes weak, the ensuing perturbation of the quantum state due to measurement becomes negligible. This has allowed probing quantum paradoxes, such as the three-box paradox [252] and quantum Cheshire cat [253] (which could be performed using OAM as suggested here [254]), and to determine average photon trajectories in superposed Gaussian beams in a model of the two-slit experiment [255], where both interferences and trajectories are observed. The correspondence between paraxial optics and Schrödinger's equation for a massive particle in two dimensions [202] make such experiments even more interesting from a fundamental point of view. Structured light is inviting to probe more complex structures of the quantum probability flux [256,257], although interpreting the optical current may be complicated [258]. In particular, a phenomenon corresponding to quantum backflow [259] is observed for OAM, whereby the interference of two light beams carrying negative orbital angular momentum results in locally occurring regions of positive angular momentum [260].

By exploiting the complex nature of weak values, weak measurements enable direct measurement of the wavefunction [261], avoiding the state reconstruction procedures of the usual quantum tomography, which become demanding in large dimensions. Structured light beams were exploited to demonstrate the reconstruction of a photon state in 27 OAM dimensions [262] (Figure 18) and of a transverse beam profile [263] (actually, structured light was also featured in direct methods [264] going beyond the standard weak measurement paradigm, such as when using strong measurements [265,266], or in combination with a wavefront restoring algorithm [267]). However, in addition to their exploitation as high-dimensional quantum systems, structured light beams connect naturally with weak measurements. Indeed, in the paradigmatic weak measurement experiment, the system is played by light polarization, while the ancilla corresponds to the spatial profile of a Gaussian beam [250] (Figure 17). Therefore, structured light is bound to play the role of advanced pointer states in the transverse position or momentum spaces. Indeed, weak measurements were demonstrated with Laguerre–Gauss and Hermite-Gauss beam pointers and modeled theoretically [268,269]. Neatly, using a Laguerre–Gauss beam as a pointer

enables the direct observation of the stereographic projection of the polarization quantum state in the pointer final position [270] (Figure 19), including the case of density matrices describing partially polarized states [270]. This method measures the concurrence of entangled qubits [271] as well. With Hermite-Gauss beam pointers, higher modes provide increased sensitivity compared to Gaussian profiles [272] and improve the estimation of small parameters [273]. Using structured-light pointers, weak measurements exploiting amplification determined extremely small rotations with high sensitivity [272,274]. Weak value amplification occurs for nearly orthogonal pre- and post-selected states, as the weak value (5) becomes very large then (the weak value denominator is the state overlap); accordingly, the observed pointer shift becomes large as well. The small rotation measured in [272] is nicely mapped to a large, amplified rotation of the spatial profile of the pointer, shaped as a small angular sector in this case. Weak measurements with Laguerre–Gauss beams offer the advantage of allowing the measurement of joint observables (without a nonlinear Hamiltonian) [275–277] and of higher moments of single particle observables [278], which is not possible with Gaussian beams. Interestingly, the imaginary part of the weak value under amplification conditions can be determined from the spatial profile of a pointer carrying OAM [278], while, with Gaussian beams, only the transverse wavevector profile can provide this information through the pointer conjugate variable [250]. Conversely, we can also weakly measure the OAM of a beam [279,280] and visualize it directly on the beam profile (interestingly, the result is linked to the argument of the weak value [281–283], a fact that does not seem to have been pointed out explicitly, to our knowledge). Actually, weak measurements can identify both indices of Laguerre–Gauss beams [284,285]. An alternative procedure exploiting optical differentiation in combination with weak measurements [286] was recently used to determine the OAM of Laguerre–Gauss beams from the post-selected beam profile [287] (i.e., without averaging the meter observable).

The connection between weak measurements and structured light formally goes deeper, on both sides of the quantum–classical frontier. Indeed, the reflection of light beams at interfaces exhibit tiny deviations from the laws of geometrical optics, when naively applying these laws to the beam axis: both angular and spatial deviations appear, known as Goos-Hänchen shifts (for longitudinal deviations, in the incidence plane) and Imbert-Fedorov shifts (for transverse deviations) [288]. In transmission, the spin Hall effect of light occurs [289], where opposite circular polarizations of light propagate slightly shifted from one another, following conservation of angular momentum. These effects are typically of the order of the wavelength or less and are thus not immediately observable. However, in a pre- and post-selected measurement, these shifts can be evidenced by weak value amplification [290–293] (with a formal analogy pointed out by Dennis and Götte [294]). Thus, the intricacies of the reflection and refraction of structured light beams [295–297] can be probed by weak measurements of the polarization for the four spatial and angular Goos-Hänchen and Imbert-Fedorov shifts [277,296,298,299], as well as for the spin Hall effect of light [300,301]. Here, the weak system–pointer interaction comes from the weak coupling linking the photon polarization and wavevectors in connection to the amplitude and phase of the reflection and transmission coefficients [288,294,302]. These effects can also be described in terms of geometric phases (of the Pancharatnam-Berry type) [288,289,303]. We note that weak value amplification is not a cure-all miracle, as the price to pay is vanishing post-selection success. However, the amplification advantages remain when facing technical limitations [250,304]. Such weak measurements of light beams and photons have a dual description [288,294,302] that can be useful to explore the quantum to classical transition. Beyond fundamental quantum optical aspects, the interaction of structured light at interfaces may be useful for metrology and sensing as it is very sensitive to the refractive index [305–309], with further improvements in sensitivity to expect from exploiting higher-order modes of structured light [272,273,277,296,298–301].

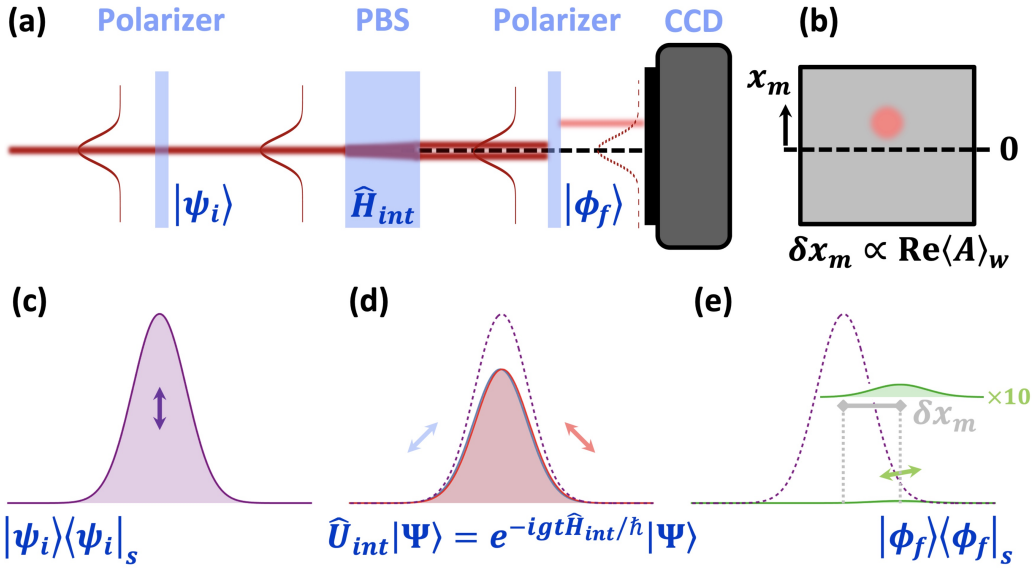

Figure 17. Principles of a weak measurement. (**a**,**c**) The measured quantum system, here the photon polarization, is pre-selected in the state $|\psi_i\rangle$ by a projective measurement $|\psi_i\rangle\langle\psi_i|_s$ applied on the system, using a polarizer. The quantum meter, here the transverse profile of the photon wavepacket, is initially in a spatial Gaussian mode $|G(x)\rangle$ centered on 0. The center of the meter profile propagates along the red line. The full quantum state of system–meter pair is $|\Psi\rangle = |\psi_i\rangle \otimes |G(x)\rangle$. (**a**,**d**) The photon passes through a birefringent plate (PBS) that, for a very short time t, weakly couples the photon propagation direction to its polarization through the interaction Hamiltonian $\hat{H}_{int} = g\hbar\hat{A}_s \otimes \hat{p}_m$, where $\hat{p}_m$ is the meter momentum, while $\hat{A}_s$ is the polarization observable weakly measured and g represents the small coupling constant. For example, we could choose $|\psi_i\rangle = |V\rangle$ as the initial state and the Pauli operator $\hat{\sigma}_x$ as the weakly measured polarization observable. The unitary evolution $\hat{U}_{int} \approx 1 - igt\hat{A}_s \otimes \hat{p}_m$ entangles the polarization and the transverse profile of the beam. As the coupling is weak ($gt \ll 1$), the two orthogonal polarizations (in our example, $|D\rangle$ and $|A\rangle$, the eigenvectors of $\hat{\sigma}_x$) are very slightly shifted—imperceptibly—in position; however, the two associated Gaussian profiles cannot interfere as their polarizations are orthogonal. (**a**,**e**) Then, we proceed to the post-selection of the system, performing a projective measurement $\left|\phi_f\right\rangle\left\langle\phi_f\right|_s$ with the last polarizer. Often, one chooses $\left\langle\phi_f|\psi_i\right\rangle \approx \epsilon$ with $\epsilon \ll 1$, so that the weak value (5) is amplified by the small parameter ϵ in the denominator (corresponding to a nearly horizontal polarization in our example $\left|\phi_f\right\rangle = |H + \epsilon\rangle$). In return, the post-selection success probability decreases as ϵ^2. After the post-selection projection, the shifted Gaussian profiles can interfere and the remaining beam centroid is shifted by a quantity related to the weak value (5): the shift is proportional to the real part of the weak value if we measure the meter position $\hat{x}_m$ and to the imaginary part if we measure the meter momentum $\hat{p}_m$. The observed shift δx_m can become anomalously large (pink direction of propagation: **a**,**b**), as the weak value can become much larger than the eigenvalues of the weakly measured observable $\hat{A}_s$. The weak value appears as a consequence of the linearization of the unitary $\hat{U}_{int}$ in the weak coupling approximation.

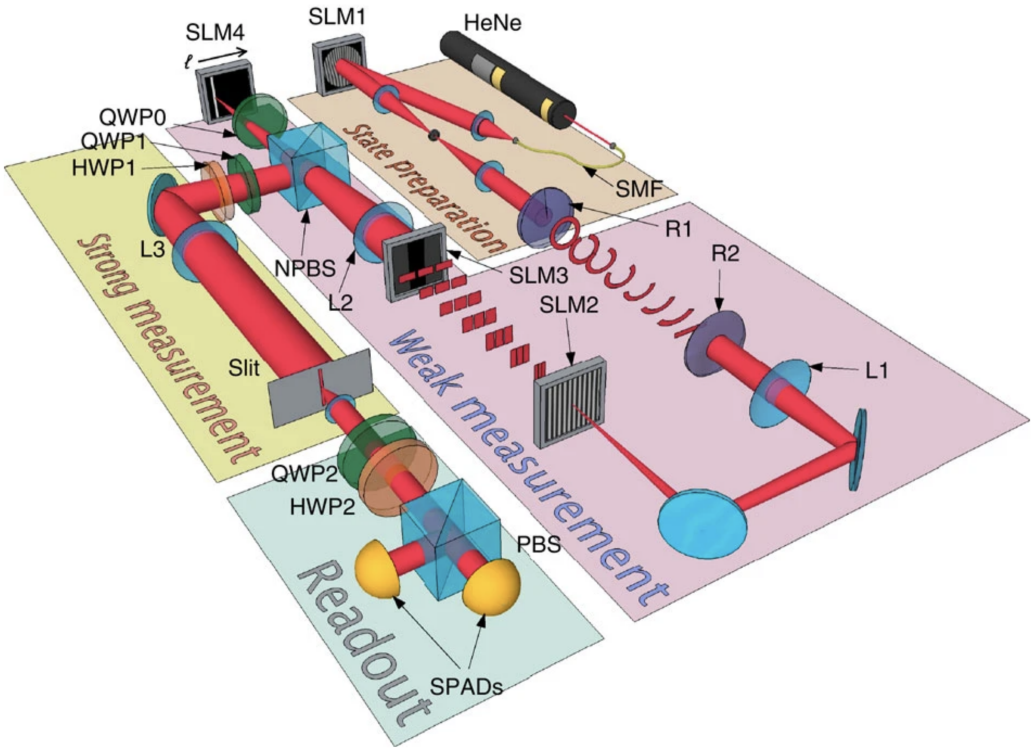

Figure 18. Experimental set-up enabling the direct measurement of a 27-dimensional OAM quantum state of photons from an attenuated HeNe beam. The state preparation generates an OAM state $|\psi_i\rangle = \sum_\ell c_\ell |\ell\rangle$ ($|\ell| \leq 13$) of vertical polarization $|V\rangle$, using a spatial light modulator (SLM1) after spatial filtering (SMF). The beam polarization corresponds to the meter. The system state is expressible in terms of weak values of projectors $\hat{\pi}_\ell = |\ell\rangle\langle\ell|$ on angular momentum basis states: $|\psi_i\rangle = k \sum_\ell \langle \pi_\ell \rangle_w |\ell\rangle$, where $k = \langle\theta_0|\psi_i\rangle / \langle\theta_0|\ell\rangle$ is a normalization constant. The post-selected state $\left|\phi_f\right\rangle = |\theta_0\rangle$ is the angular position basis state $\theta_0 = 0$ (the $|\ell\rangle$ and $|\theta\rangle$ are mutually unbiased bases, ensuring that k does not depend on ℓ for $\theta_0 = 0$). To perform the weak measurements of the projectors $\hat{\pi}_\ell$, the OAM modes with azimuthal phase $e^{i\ell\varphi}$ are first transformed to momentum modes with spatial phase $e^{i\ell x/a}$ using two custom refractive elements (R1 and R2). These different momentum modes are focused on different x positions on SLM4. SLM2 and SLM3 improve the mode resolution obtained on SLM4 (SLM2 is a fan-out element that diffracts three copies of each momentum mode, while SLM3 performs a relative-phase correction between the copies). A projector $\hat{\pi}_\ell$ is weakly probed by rotating the polarization of the associated OAM mode by a small angle α (using SLM4 and the quarter-wave plate QWP0). Post-selection on $|\theta_0\rangle$ is performed by passing the beam through a 10 µm slit placed in the Fourier plane of the lens L3 (as SLM4 and the slit are in conjugated planes, the positions x in those planes represent $|\ell\rangle$ and $|\theta\rangle$, respectively). Finally, the meter is read out by counting the photons at the two exits of a polarizing beamsplitter (PBS) using single-photon avalanche detectors (SPAD). If we note the final meter state $\left|\mu_f\right\rangle$, then measuring the polarization in the $\{|D\rangle, |A\rangle\}$ diagonal basis gives the real part of the OAM weak value, while measuring it in the circular polarization basis $\{|R\rangle, |L\rangle\}$ provides the imaginary part because $\left\langle \mu_f | \hat{\sigma}_x - i\hat{\sigma}_y | \mu_f \right\rangle = \sin\alpha \langle \pi_\ell \rangle_w$ at the end of the post-selected weak measurement [262]. Reproduced with permission from SNCSC.

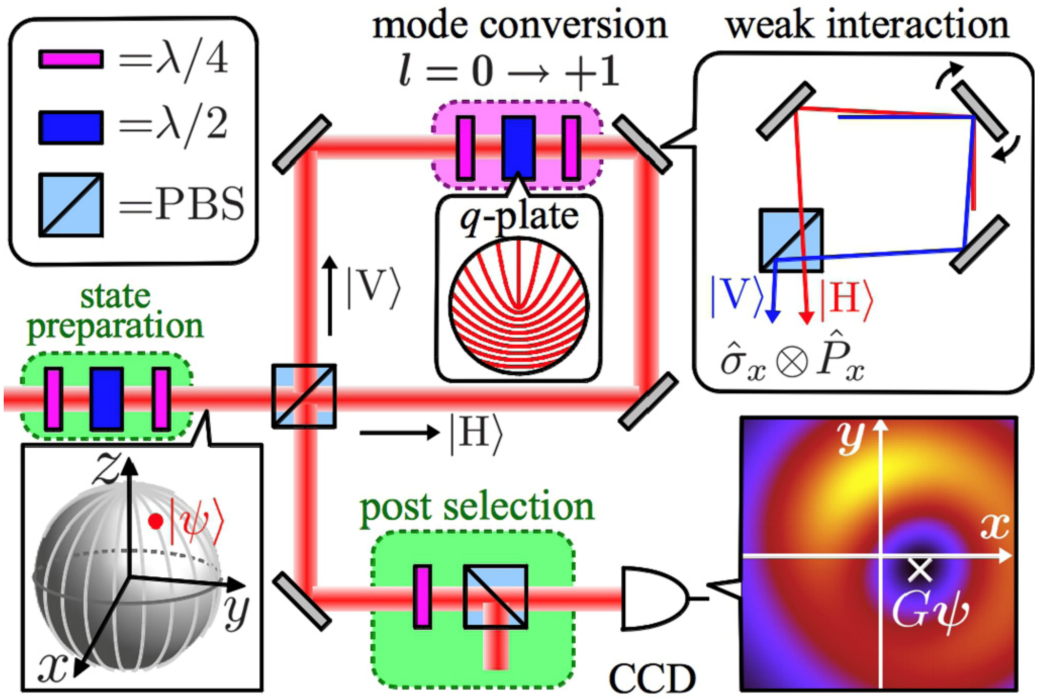

Figure 19. Stereographic visualization of a polarization state using weak measurements with a vortex beam [270]. An arbitrary polarization state $|\psi\rangle = \cos(\theta/2)|H\rangle + \sin(\theta/2)e^{i\varphi}|V\rangle$ of a Gaussian beam is pre-selected. Then, a Sagnac interferometer with a q-plate converts the Gaussian mode to a Laguerre–Gauss mode ($\ell = 1$), without affecting the beam polarization when optimally aligned. The $|H\rangle$ and $|V\rangle$ components of the beam rotate in opposite directions due to the polarizing beamsplitter (PBS) at the entrance of the interferometer. A small rotation of a mirror detunes slightly the interferometer so that the $\hat{\sigma}_x$ polarization observable couples weakly to the Gaussian beam momentum $\hat{p}_x$. After exiting the interferometer, the beam polarization is post-selected on $|V\rangle$. The weak value equals $\langle\hat{\sigma}_x\rangle_w = \langle H|\hat{\sigma}_x|\psi\rangle / \langle H|\psi\rangle = \tan(\theta/2)e^{i\varphi} = \cot\theta' e^{i\varphi}$, where θ' is now the angle seen from the pole of the sphere (between the z axis and the line joining the north pole to the state on the Bloch sphere). The weak value is thus the stereographic projection of the state on the complex plane $z = 0$ (with x corresponding to the real axis and y the imaginary axis). The position of the beam vortex after successful post-selection is shifted proportionally to the real part of the weak value along the x axis and to the imaginary part of the weak value along the y axis, enabling the visualization of the stereographic projection of the initial, arbitrary polarization state. Reprinted figure with permission from [270] ©2014 by the American Physical Society.

6. Conclusions

In this perspective article, we present the theoretical background of structured light and the properties of a few beams interesting for broad and conceivable applications in photonics, sensing, chirality, holography, and quantum technology. Structured light profoundly connects the topology of light with matter and its responses, and uniquely interconnects fundamental physics with quantum information science. The essential elements of structured light are not only their exceptional topology (quite different from the plane waves) or their nondiffraction capability but also the presence of nonseparable local correlations. We discussed in detail the importance of structured light, including in the presence of entanglement (nonseparable correlations of their degrees of freedom), for various classical and quantum applications. The opportunity to design and control different topologies of light on command will lead to a new scientific and technological revolution. It can improve quantum measurements, impacting optics and quantum physics at both the fundamental and applied levels. It can help the design and study of original complex materials, such as chiral and topological super- and semiconductors. It can steer chemical and biological dynamics and affect chemical reactivity, with remarkable control, just by shaping the light

topology. Furthermore, engineering and controlling structured light will rapidly lead to new surface optics, nanoscale optics, and photonics breakthroughs. Even though, at the moment, the interaction of structured light with matter is still under rapid development, this highlight aims primarily to capture the attention of the wider physical and quantum science community for structured light and its power. Ultimately, the structured light unifies many ideas and perspectives in physics and material science and uniquely connects geometry with physics. Harnessing the power of structured light is essential for future scientific and technological advancement.

Author Contributions: Conceptualization: B.K.; project administration: B.B. and B.K.; original draft preparation: B.B., Y.d.C., M.A.F., T.V., Y.C. and B.K.; writing—review and editing: B.B., Y.d.C., M.A.F., T.V., Y.C. and B.K.; visualization: B.B.; funding acquisition: B.B., Y.d.C., M.A.F., T.V., Y.C. and B.K. All authors have read and agreed to the published version of the manuscript.

Funding: BB and BK acknowledge funding provided by the Institute of Physics Belgrade, through the institutional funding by the Ministry of Science, Technological Development and Innovations of the Republic of Serbia, and the support of the Office of Naval Research Global through the Research Grant N62902-22-1-2024. YdC acknowledges the fund for scientific research—Flanders for a junior post-doc position (nr 1234222N). MAF acknowledges financial support from ESA MAP Project (4000129503/20/NL/PG/pt): Wound Healing In Space: Key challenges towards Intelligent and Enabling Sensing platforms (WHISKIES). TV acknowledges financial support from KULeuven. This work was supported by the Action de Recherche Concertée WeaM at the University of Namur (19/23-001). BB, MAF, TV, YC, and BK acknowledge the support of the EU: the EIC Pathfinder Challenges 2022 call through the Research Grant 101115149 (project ARTEMIS).

Data Availability Statement: The data that supports the findings of this study are available within the article.

Acknowledgments: All authors warmly acknowledge fruitful discussion and contribution of Dragana Jović Savić from the Institute of Physics Belgrade and Dejan Timotijević from the Institute of Multidisciplinary Research Belgrade regarding the physics of nondiffracting beams. BB and BK acknowledge funding provided by the Institute of Physics Belgrade, through the institutional funding by the Ministry of Science, Technological Development and Innovations of the Republic of Serbia, and the support of the Office of Naval Research Global through the Research Grant N62902-22-1-2024. Additionally, BK acknowledges support from F.R.S.-FNRS. YdC acknowledges the fund for scientific research-Flanders for a junior post-doc position (nr 1234222N). MAF acknowledges financial support from ESA MAP Project (4000129503/20/NL/PG/pt): Wound Healing In Space: Key challenges towards Intelligent and Enabling Sensing platforms (WHISKIES). TV acknowledges financial support from KULeuven. YC is a Research Associate of the Fund for Scientific Research F.R.S.-FNRS. This work was supported by the Action de Recherche Concertée WeaM at the University of Namur (19/23-001). BB, MAF, TV, YC, and BK acknowledge the support of the EU: the EIC Pathfinder Challenges 2022 call through the Research Grant 101115149 (project ARTEMIS). The content reflects only the authors' views, and the European Commission is not responsible for any use that may be made of the information it contains.

Conflicts of Interest: The authors declare no conflicts of interest.

References

1. Haroche, S.; Raimond, J.-M. *Exploring the Quantum: Atoms, Cavities and Photons*; Oxford University Press: Oxford, UK, 2006.
2. Secor, J.; Alfano, R.; Ashrafi, S. *Complex Light*; IOP: Bristol, UK, 2017. [CrossRef]
3. Zangwill, A. *Modern Elecromagnetism*; Cambridge University Press: Cambridge, UK, 2013. [CrossRef]
4. Rubinsztein-Dunlop, H.; Forbes, A.; Berry, M.V.; Dennis, M.R.; Andrews, D.L.; Mansuripur, M.; Denz, C.; Alpmann, C.; Banzer, P.; Bauer, T.; et al. Roadmap on structured light. *J. Opt.* **2017**, *19*, 013001. [CrossRef]
5. Bliokh, K.Y.; Karimi, E.; Padgett, M.J.; Alonso, M.A.; Dennis, M.R.; Dudley, A.; Forbes, A.; Zahedpour, S.; Hancock, S.W.; Milchberg, H.M.; et al. Roadmap on structured waves. *J. Opt.* **2023**, *25*, 103001. [CrossRef]
6. Wang, J.; Castellucci, F.; Franke-Arnold, S. Vectorial light-matter interaction: Exploring spatially structured complex light fields. *AVS Quantum Sci.* **2020**, *2*, 031702. [CrossRef]
7. Forbes, A.K.; Andrews, D.L. Orbital angular momentum of twisted light: Chirality and optical activity. *J. Phys. Photonics* **2021**, *3*, 022007. [CrossRef]
8. Frankel, T. *The Geometry of Physics*; Cambridge University Press: Cambridge, UK, 2004. [CrossRef]

9. Durnin, J.; Miceli, J.J.; Eberly, J.H. Diffraction-free beams. *Phys. Rev. Lett.* **1987**, *58*, 1499–1501. [CrossRef] [PubMed]
10. Durnin, J. Exact solutions for nondiffracting beams. I. The scalar theory. *J. Opt. Soc. Am. A* **1987**, *4*, 651–654. [CrossRef]
11. Boguslawski, M.; Rose, P.; Denz, C. Increasing the structural variety of discrete nondiffracting wave fields. *Phys. Rev. A* **2011**, *84*, 013832. [CrossRef]
12. Rose, P.; Boguslawski, M.; Denz, C. Nonlinear lattice structures based on families of complex nondiffracting beams. *New J. Phys.* **2012**, *14*, 033018. [CrossRef]
13. McQueen, C.; Arlt, J.; Dholakia, K. An experiment to study a "nondiffracting" light beam. *Am. J. Phys.* **1999**, *67*, 912–915. [CrossRef]
14. Gutiérrez-Vega, J.C.; Iturbe-Castillo, M.D.; Chávez-Cerda, S. Alternative formulation for invariant optical fields: Mathieu beams. *Opt. Lett.* **2000**, *25*, 1493–1495. [CrossRef]
15. Bandres, M.A.; Gutiérrez-Vega, J.C.; Chávez-Cerda, S. Parabolic nondiffracting optical wave fields. *Opt. Lett.* **2004**, *29*, 44–46. [CrossRef]
16. Freedman, B.; Bartal, G.; Segev, M.; Lifshitz, R.; Christodoulides, D.N.; Fleischer, J.W. Wave and defect dynamics in nonlinear photonic quasicrystals. *Nature* **2006**, *440*, 04722. [CrossRef]
17. Vicente, O.C.; Caloz, C. Bessel beams: A unified and extended perspective. *Optica* **2021**, *8*, 2334–2536. [CrossRef]
18. Boguslawski, M.; Lučić, N.M.; Diebel, F.; Timotijević, D.V.; Denz, C.; Savić, D.M.J. Light localization in optically induced deterministic aperiodic Fibonacci lattices. *Optica* **2016**, *3*, 711–717. [CrossRef]
19. Lóxpez-Mariscal, C.; Gutiérrez-Vega, J.C.; Milne, G.; Dholakia, K. Orbital angular momentum transfer in helical Mathieu beams. *Opt. Express* **2006**, *14*, 4182–4187. [CrossRef] [PubMed]
20. Baumgartl, J.; Mazilu, M.; Dholakia, K. Optically mediated particle clearing using Airy wavepackets. *Nat. Photonics* **2008**, *2*, 675–678. [CrossRef]
21. Fleischer, J.; Segev, M.; Efremidis, N.; Christodoulides, D. Observation of two-dimensional discrete solitons in optically induced nonlinear photonic lattices. *Nature* **2003**, *422*, 147. [CrossRef]
22. Sogomonian, S.; Klewitz, S.; Herminghaus, S. Self-reconstruction of a Bessel beam in a nonlinear medium. *Opt. Commun.* **1997**, *139*, 313–319. [CrossRef]
23. Bouchal, Z.; Wagner, J.; Chlup, M. Self-reconstruction of a distorted nondiffracting beam. *Opt. Commun.* **1998**, *151*, 207–211. [CrossRef]
24. Chávez-Cerda, S.; Meneses-Nava, M.A.; Hickmann, J.M. Interference of traveling nondiffracting beams. *Opt. Lett.* **1998**, *23*, 1871–1873. [CrossRef]
25. Vasara, A.; Turunen, J.; Friberg, A.T. Realization of general nondiffracting beams with computer-generated holograms. *J. Opt. Soc. Am. A* **1989**, *6*, 1748–1754. [CrossRef] [PubMed]
26. Scott, G.; McArdle, N. Efficient generation of nearly diffraction-free beams using an axicon. *Opt. Eng.* **1992**, *31*, 2640. [CrossRef]
27. Chattrapiban, N.; Rogers, E.A.; Cofield, D.; Wendell, T.; Hill, I.; Roy, R. Generation of nondiffracting Bessel beams by use of a spatial light modulator. *Opt. Lett.* **2003**, *28*, 2183–2185. [CrossRef] [PubMed]
28. Berry, M.V.; Balazs, N.L. Nonspreading wave packets. *Am. J. Phys.* **1979**, *47*, 264. [CrossRef]
29. Siviloglou, G.A.; Christodoulides, D.N. Accelerating finite energy Airy beams. *Opt. Lett.* **2007**, *32*, 979–981. [CrossRef]
30. Siviloglou, G.A.; Broky, J.; Dogariu, A.; Christodoulides, D.N. Observation of Accelerating Airy Beams. *Phys. Rev. Lett.* **2007**, *99*, 213901. [CrossRef] [PubMed]
31. Siviloglou, G.A.; Broky, J.; Dogariu, A.; Christodoulides, D.N. Ballistic dynamics of Airy beams. *Opt. Lett.* **2008**, *33*, 207–209. [CrossRef] [PubMed]
32. Bandres, M.A.; Kaminer, I.; Mills, M.; Rodríguez-Lara, B.; Greenfield, E.; Segev, M.; Christodoulides, D.N. Accelerating Optical Beam. *Opt. Photonics News* **2013**, *24*, 30–37. [CrossRef]
33. Besieris, I.M.; Shaarawi, A.M. A note on an accelerating finite energy Airy beam. *Opt. Lett.* **2007**, *32*, 2447–2449. [CrossRef]
34. Novitsky, A.V.; Novitsky, D.V. Nonparaxial Airy beams: Role of evanescent waves. *Opt. Lett.* **2009**, *34*, 3430–3432. [CrossRef]
35. Mathis, A.; Courvoisier, F.; Froehly, L.; Furfaro, L.; Jacquot, M.; Lacourt, P.A.; Dudley, J.M. Micromachining along a curve: Femtosecond laser micromachining of curved profiles in diamond and silicon using accelerating beams. *Appl. Phys. Lett.* **2012**, *101*, 071110. [CrossRef]
36. Chong, A.; Renninger, W.H.; Christodoulides, D.N.; Wise, F.W. Airy-Bessel wave packets as versatile linear light bullets. *Nat. Photonics* **2010**, *4*, 103–106. [CrossRef]
37. Zhang, P.; Wang, S.; Liu, Y.; Yin, X.; Lu, C.; Chen, Z.; Zhang, X. Plasmonic Airy beams with dynamically controlled trajectories. *Opt. Lett.* **2011**, *36*, 3191–3193. [CrossRef] [PubMed]
38. Minovich, A.; Klein, A.E.; Janunts, N.; Pertsch, T.; Neshev, D.N.; Kivshar, Y.S. Generation and Near-Field Imaging of Airy Surface Plasmons. *Phys. Rev. Lett.* **2011**, *107*, 116802. [CrossRef]
39. Polynkin, P.; Kolesik, M.; Moloney, J.V.; Siviloglou, G.A.; Christodoulides, D.N. Curved Plasma Channel Generation Using Ultraintense Airy Beams. *Science* **2009**, *324*, 229–232. [CrossRef]
40. Ellenbogen, T.; Voloch-Bloch, N.; Ganany-Padowicz, A.; Arie, A. Nonlinear generation and manipulation of Airy beams. *Nat. Photon.* **2009**, *3*, 395–398. [CrossRef]
41. Broky, J.; Siviloglou, G.A.; Dogariu, A.; Christodoulides, D.N. Self-healing properties of optical Airy beams. *Opt. Express* **2008**, *16*, 12880–12891. [CrossRef]

42. Efremidis, N.K. Airy trajectory engineering in dynamic linear index potentials. *Opt. Lett.* **2011**, *36*, 3006–3008. [CrossRef] [PubMed]
43. Efremidis, N.K. Accelerating beam propagation in refractive-index potentials. *Phys. Rev. A* **2014**, *89*, 023841. [CrossRef]
44. Makris, K.G.; Kaminer, I.; El-Ganainy, R.; Efremidis, N.K.; Chen, Z.; Segev, M.; Christodoulides, D.N. Accelerating diffraction-free beams in photonic lattices. *Opt. Lett.* **2014**, *39*, 2129–2132. [CrossRef]
45. Chávez-Cerda, S.; Ruiz, U.; Arrizón, V.; Moya-Cessa, H.M. Generation of Airy solitary-like wave beams by acceleration control in inhomogeneous media. *Opt. Express* **2011**, *19*, 16448–16454. [CrossRef]
46. Lučić, N.M.; Bokić, B.M.; Grujić, D.i.c.v.; Pantelić, D.V.; Jelenković, B.M.; Piper, A.; Jović, D.M.; Timotijević, D.V. Defect-guided Airy beams in optically induced waveguide arrays. *Phys. Rev. A* **2013**, *88*, 063815. [CrossRef]
47. Diebel, F.; Bokić, B.M.; Boguslawski, M.; Piper, A.; Timotijević, D.V.; Jović, D.M.; Denz, C. Control of Airy-beam self-acceleration by photonic lattices. *Phys. Rev. A* **2014**, *90*, 033802. [CrossRef]
48. Rose, P.; Diebel, F.; Boguslawski, M.; Denz, C. Airy beam induced optical routing. *Appl. Phys. Lett.* **2013**, *102*, 101101. [CrossRef]
49. Bekenstein, R.; Segev, M. Self-accelerating optical beams in highly nonlocal nonlinear media. *Opt. Express* **2011**, *19*, 23706–23715. [CrossRef]
50. Hu, Y.; Huang, S.; Zhang, P.; Lou, C.; Xu, J.; Chen, Z. Persistence and breakdown of Airy beams driven by an initial nonlinearity. *Opt. Lett.* **2010**, *35*, 3952–3954. [CrossRef]
51. Driben, R.; Konotop, V.V.; Meier, T. Coupled Airy breathers. *Opt. Lett.* **2014**, *39*, 5523–5526. [CrossRef] [PubMed]
52. Diebel, F.; Bokić, B.M.; Timotijević, D.V.; Savić, D.M.J.; Denz, C. Soliton formation by decelerating interacting Airy beams. *Opt. Express* **2015**, *23*, 24351–24361. [CrossRef]
53. Zannotti, A.; Vasiljević, J.M.; Timotijević, D.V.; Savić, D.M.J.; Denz, C. Morphing discrete diffraction in nonlinear Mathieu lattices. *Opt. Lett.* **2019**, *44*, 1592–1595. [CrossRef]
54. Zannotti, A.; Vasiljević, J.M.; Timotijević, D.V.; Jović Savić, D.M.; Denz, C. Visualizing the Energy Flow of Tailored Light. *Adv. Opt. Mater.* **2018,** *6*, 1701355. [CrossRef]
55. Vasiljević, J.M.; Zannotti, A.; Timotijević, D.V.; Denz, C.; Savić, D.M.J. Light transport and localization in disordered aperiodic Mathieu lattices. *Opt. Lett.* **2022**, *47*, 702–705. [CrossRef] [PubMed]
56. Lakhtakia, A. (Ed.) *Selected Papers on Natural Optical Activity*; SPIE: Bellingham, WA, USA, 1990; Volume MS15.
57. Allen, L.; Beijersbergen, M.W.; Spreeuw, R.J.C.; WoerdmanDurnin, J.P. Orbital angular momentum of light and the transformation of Laguerre-Gaussian laser modes. *Phys. Rev. A.* **1992**, *45*, 8185–8189. [CrossRef] [PubMed]
58. Rosales-Guzman, C.; Ndagano, B.; Forbes, A. A review of complex vector light fields and their applications. *J. Opt.* **2018**, *20*, 123001. [CrossRef]
59. Dholakia, K.; Lee, W.M. Optical trapping takes shape: The use of structured light fields. *Adv. At. Mol. Opt. Phys.* **2008**, *56*, 261–337. [CrossRef]
60. Piccirillo, B.; Toscano, C.; Vetrano, F.; Santamato, E. Orbital and Spin Photon Angular Momentum Transfer in Liquid Crystals. *Phys. Rev. Lett.* **2001**, *86*, 2285–2288. [CrossRef] [PubMed]
61. Babiker, M.; Bennett, C.; Andrews, D.L.; Dávila Romero, L.C. Orbital Angular Momentum Exchange in the Interaction of Twisted Light with Molecules. *Phys. Rev. Lett.* **2002**, *89*, 143601. [CrossRef] [PubMed]
62. Andrews, D.L.; Dávila Romero, L.C.; Babiker, M. On optical vortex interactions with chiral matter. *Opt. Commun.* **2004**, *237*, 133–139. [CrossRef]
63. Coles, M.; Andrews, D.L. Chirality and angular momentum in optical radiation. *Phys. Rev. A* **2012**, *85*, 063810. [CrossRef]
64. Araoka, F.; Verbiest, T.; Clays, K.; Persoons, A. Interactions of twisted light with chiral molecules: An experimental investigation. *Phys. Rev. A* **2005**, *71*, 055401. [CrossRef]
65. Loeffler, W.; Broer, J.D.; Woerdman, P.J. Circular dichroism of cholesteric polymers and the orbital angular momentum of light. *Phys. Rev. A* **2011**, *83*, 065801. [CrossRef]
66. Brullot, W.; Vanbel, K.M.; Swusten, T.; Verbiest, T. Resolving enantiomers using the optical angular momentum of twisted light. *Sci. Adv.* **2016**, *2*, e1501349. [CrossRef] [PubMed]
67. Forbes, A.K.; Andrews, D.L. Optical orbital angular momentum: Twisted light and chirality. *Opt. Lett.* **2018**, *43*, 435–438. [CrossRef]
68. Forbes, A.K.; Andrews, D.L. Spin-orbit interactions and chiroptical effects engaging orbital angular momentum of twisted light in chiral and achiral media. *Phys. Rev. A* **2019**, *99*, 023837. [CrossRef]
69. Ni, J.; Liu, S.; Hu, G.; Hu, Y.; Lao, Z.; Li, J.; Zhang, Q.; Wu, D.; Dong, S.; Chu, J.; et al. Giant helical dichroism of single chiral nanostructures with photonic orbital angular momentum. *ACS Nano* **2021**, *15*, 2893–2900. [CrossRef]
70. Ni, J.; Liu, S.; Lao, Z.; Wang, Z.; Huang, K.; Ji, S.; Li, J.; Huang, Z.; Xiong, Q.; Hu, Y.; et al. Gigantic vortical differential scattering as a monochromatic probe for multiscale chiral structures. *Proc. Natl. Acad. Sci. USA* **2021**, *118*, e2020055118. [CrossRef]
71. Liu, S.; Ni, J.; Zhang, C.; Wang, X.; Cao, Y.; Wang, D.; Ji, S.; Pan, D.; Li, R.; Wu, H.; et al. Tailoring Optical Vortical Dichroism with Stereometamaterials. *Laser Photonics Rev.* **2022**, *16*, 2100518. [CrossRef]
72. Begin, J.L.; Jain, A.; Parks, A.; Hufnagel, F.; Corkum, P.; Karimi, E.; Brabec, T.; Bhardwaj, R. Nonlinear helical dichroism in chiral and achiral molecules. *Nat. Photonics* **2023**, *17*, 82–88. [CrossRef]
73. Gabor, D. A New Microscopic Principle. *Nature* **1948**, *161*, 777–778. [CrossRef]

74. Ruffato, G.; Rossi, R.; Massari, M.; Mafakheri, E.; Capaldo, P.; Romanato, F. Design, fabrication and characterization of Computer Generated Holograms for anti-counterfeiting applications using OAM beams as light decoders. *Sci. Rep.* **2017**, *7*, 18011. [CrossRef]
75. Ashley, J.; Bernal, M.P.; Burr, G.W.; Coufal, H.; Guenther, H.; Hoffnagle, J.A.; Jefferson, C.M.; Marcus, B.; MacFarlane, R.M.; Shelby, R.M.; et al. Holographic Data Storage Technology. *IBM J. Res. Dev.* **2000**, *44*, 341–368. [CrossRef]
76. Kosma, K.; Andrianakis, M.; Hatzigiannakis, K.; Tornari, V. Digital holographic interferometry for cultural heritage structural diagnostics: A coherent and a low-coherence optical set-up for the study of a marquetry sample. *Strain* **2018**, *54*, e12263. [CrossRef]
77. Coppola, G.; Zito, G.; Luca, A.C.D.; Ferrara, M.A. Polarized Digital Holography as Valuable Analytical Tool in Biological and Medical Research. In *Proceedings of the Digital Holography and Three-Dimensional Imaging 2019*; Paper Th4A.5; Optica Publishing Group: Washington, DC, USA, 2019. [CrossRef]
78. Wang, J.; Liang, Y. Generation and Detection of Structured Light: A Review. *Front. Phys.* **2021**, *9*, 688284. [CrossRef]
79. Hariharan, P. *Basics of Holography*; Cambridge University Press: Cambridge, UK, 2002. [CrossRef]
80. Stoykova, E.; Kang, H.; Park, J. Twin-image problem in digital holography-a survey (Invited Paper). *Chin. Opt. Lett.* **2014**, *12*, 060013. [CrossRef]
81. Tahara, T.; Lee, Y.; Ito, Y.; Xia, P.; Shimozato, Y.; Takahashi, Y.; Awatsuji, Y.; Nishio, K.; Ura, S.; Kubota, T.; et al. Superresolution of interference fringes in parallel four-step phase-shifting digital holography. *Opt. Lett.* **2014**, *39*, 1673–1676. [CrossRef] [PubMed]
82. Guo, C.S.; Cheng, X.; Ren, X.Y.; Ding, J.P.; Wang, H.T. Optical vortex phase-shifting digital holography. *Opt. Express* **2004**, *12*, 5166–5171. [CrossRef]
83. Zhang, X.; Zhang, J.; Li, Y.; Zhou, S.; Liu, D.; Zhu, J. Phase-shifting digital holography with vortex beam in one single exposure. *Optik* **2019**, *185*, 1024–1029. [CrossRef]
84. Zhang, X.; Zhang, J.; Zhou, S.; Liu, D.; Zhu, J. Single-shot phase-shifting digital holography with amplitude-only Fermat-spiral sieves. *Laser Phys. Lett.* **2019**, *16*, 025002. [CrossRef]
85. Born, M.; Wolf, E.; Bhatia, A.B.; Clemmow, P.C.; Gabor, D.; Stokes, A.R.; Taylor, A.M.; Wayman, P.A.; Wilcock, W.L. *Principles of Optics: Electromagnetic Theory of Propagation, Interference and Diffraction of Light*, 7th ed.; Cambridge University Press: Cambridge, UK, 1999. [CrossRef]
86. Gustafsson, M.G.L. Surpassing the lateral resolution limit by a factor of two using structured illumination microscopy. *J. Microsc.* **2001**, *198*, 82–87. [CrossRef]
87. Mudassar, A.A.; Hussain, A. Super-resolution of active spatial frequency heterodyning using holographic approach. *Appl. Opt.* **2010**, *49*, 3434–3441. [CrossRef]
88. Gao, P.; Pedrini, G.; Osten, W. Structured illumination for resolution enhancement and autofocusing in digital holographic microscopy. *Opt. Lett.* **2013**, *38*, 1328–1330. [CrossRef] [PubMed]
89. Shin, S.; Kim, K.; Yoon, J.; Park, Y. Active illumination using a digital micromirror device for quantitative phase imaging. *Opt. Lett.* **2015**, *40*, 5407–5410. [CrossRef] [PubMed]
90. Ganjkhani, Y.; Charsooghi, M.A.; Akhlaghi, E.A.; Moradi, A.R. Super-resolved Mirau digital holography by structured illumination. *Opt. Commun.* **2017**, *404*, 110–117. [CrossRef]
91. Meng, Z.; Pedrini, G.; Lv, X.; Ma, J.; Nie, S.; Yuan, C. DL-SI-DHM: A deep network generating the high-resolution phase and amplitude images from wide-field images. *Opt. Express* **2021**, *29*, 19247–19261. [CrossRef] [PubMed]
92. Ren, H.; Briere, G.; Fang, X.; Ni, P.; Sawant, R.; Héron, S.; Chenot, S.; Vézian, S.; Damilano, B.; Brändli, V.; et al. Metasurface orbital angular momentum holography. *Nat. Commun.* **2019**, *10*, 2986. [CrossRef] [PubMed]
93. Ren, H.; Fang, X.; Jang, J.; Bürger, J.; Rho, J.; Maier, S.A. Complex-amplitude metasurface-based orbital angular momentum holography in momentum space. *Nat. Nanotechnol.* **2020**, *15*, 948–955. [CrossRef] [PubMed]
94. Fang, X.; Ren, H.; Gu, M. Orbital angular momentum holography for high-security encryption. *Nat. Photonics* **2020**, *14*, 101–108. [CrossRef]
95. Zhou, H.; Sain, B.; Wang, Y.; Schlickriede, C.; Zhao, R.; Zhang, X.; Wei, Q.; Li, X.; Huang, L.; Zentgraf, T. Polarization-Encrypted Orbital Angular Momentum Multiplexed Metasurface Holography. *ACS Nano* **2020**, *14*, 5553–5559. [CrossRef] [PubMed]
96. Trajtenberg-Mills, S.; Juwiler, I.; Arie, A. On-axis shaping of second-harmonic beams. *Laser Photonics Rev.* **2015**, *9*, L40–L44. [CrossRef]
97. Fang, X.; Yang, H.; Yao, W.; Wang, T.; Zhang, Y.; Gu, M.; Xiao, M. High-dimensional orbital angular momentum multiplexing nonlinear holography. *Adv. Photonics* **2021**, *3*, 015001. [CrossRef]
98. Töpfer, S.; Basset, M.G.; Fuenzalida, J.; Steinlechner, F.; Torres, J.P.; Gräfe, M. Quantum holography with undetected light. *Sci. Adv.* **2022**, *8*, eabl4301. [CrossRef]
99. He, L.; Liu, K.; He, Z.; Cao, L. Three-dimensional holographic communication system for the metaverse. *Opt. Commun.* **2023**, *526*, 128894. [CrossRef]
100. Aiello, A.; Töppel, F.; Marquardt, C.; Giacobino, E.; Leuchs, G. Quantum-like nonseparable structures in optical beams. *New J. Phys.* **2015**, *17*, 043024. [CrossRef]
101. Forbes, A.; Aiello, A.; Ndagano, B. Classically entangled light. *Prog. Opt.* **2019**, *64*, 99–153. [CrossRef]
102. Goldstein, D. *Polarized Light, Revised and Expanded*, 2nd ed.; Marcel Dekker Inc.: New York, NY, USA, 2003. [CrossRef]
103. Bengtsson, I.; Zyczkowski, K. *Geometry of Quantum States*; Cambridge University Press: Cambridge, UK, 2009. [CrossRef]
104. Saito, S. Photonic quantum chromodynamics. *Front. Phys.* **2023**, *11*, 1225488. [CrossRef]

105. Padgett, M.J.; Courtial, J. Poincaré-sphere equivalent for light beams containing orbital angular momentum. *Opt. Lett.* **1999**, *24*, 430–432. [CrossRef]
106. Milione, G.; Sztul, H.I.; Nolan, D.A.; Alfano, R.R. Higher-order Poincaré sphere, Stokes parameters, and the angular momentum of light. *Phys. Rev. Lett.* **2011**, *107*, 053601. [CrossRef]
107. Milione, G.; Evans, S.; Nolan, D.A.; Alfano, R.R. Higher order Pancharatnam-Berry phase and the angular momentum of light. *Phys. Rev. Lett.* **2012**, *108*, 190401. [CrossRef]
108. Yang, L.P. Geometric phase for twisted light. *Opt. Express* **2023**, *31*, 10287–10296. [CrossRef]
109. Gutiérrez-Cuevas, R.; Dennis, M.R.; Alonso, M.A. Generalized Gaussian beams in terms of Jones vectors. *J. Opt.* **2019**, *21*, 084001. [CrossRef]
110. Dennis, M.R.; Alonso, M.A. Gaussian mode families from systems of rays. *J. Phys. Photonics* **2019**, *1*, 025003. [CrossRef]
111. Gutiérrez-Cuevas, R.; Wadood, S.A.; Vamivakas, A.N.; Alonso, M.A. Modal Majorana sphere and hidden symmetries of structured-Gaussian beams. *Phys. Rev. Lett.* **2020**, *125*, 123903. [CrossRef] [PubMed]
112. Shen, Y.; Wang, Z.; Fu, X.; Naidoo, D.; Forbes, A. SU(2) Poincaré sphere: A generalized representation for multidimensional structured light. *Phys. Rev. A* **2020**, *102*, 031501(R). [CrossRef]
113. Shen, Y. Rays, waves, SU(2) symmetry and geometry: Toolkits for structured light. *J. Opt.* **2021**, *23*, 124004. [CrossRef]
114. Zhang, H.; Zeng, J.; Lu, X.; Wang, Z.; Zhao, C.; Cai, Y. Review on fractional vortex beam. *Nanophotonics* **2022**, *11*, 241–273. [CrossRef]
115. Götte, J.B.; Franke-Arnold, S.; Zambrini, R.; Barnett, S.M. Quantum formulation of fractional orbital angular momentum. *J. Mod. Opt.* **2007**, *54*, 1723–1738. [CrossRef]
116. Oemrawsingh, S.S.R.; Ma, X.; Voigt, D.; Aiello, A.; Eliel, E.R.; 't Hooft, G.W.; Woerdman, J.P. Experimental demonstration of fractional orbital angular momentum Entanglement of two photons. *Phys. Rev. Lett.* **2005**, *95*, 240501. [CrossRef] [PubMed]
117. Sit, A.; Bouchard, F.; Fickler, R.; Gagnon-Bischoff, J.; Larocque, H.; Heshami, K.; Elser, D.; Peuntinger, C.; Günthner, K.; Heim, B.; et al. High-dimensional intracity quantum cryptography with structured photons. *Optica* **2017**, *4*, 1006–1010. [CrossRef]
118. Bouchard, F.; Fickler, R.; Boyd, R.W.; Karimi, E. High-dimensional quantum cloning and applications to quantum hacking. *Sci. Adv.* **2017**, *3*, e1601915. [CrossRef]
119. Ndagano, B.; Perez-Garcia, B.; Roux, F.S.; McLaren, M.; Rosales-Guzman, C.; Zhang, Y.; Mouane, O.; Hernandez-Aranda, R.I.; Konrad, T.; Forbes, A. Characterizing quantum channels with non-separable states of classical light. *Nat. Phys.* **2017**, *13*, 397–402. [CrossRef]
120. Nape, I.; Singh, K.; Klug, A.; Buono, W.; Rosales-Guzman, C.; McWilliam, A.; Franke-Arnold, S.; Kritzinger, A.; Forbes, P.; Dudley, A.; et al. Revealing the invariance of vectorial structured light in complex media. *Nat. Photonics* **2022**, *16*, 538–546. [CrossRef]
121. Sekga, C.; Mafu, M. Measurement device-independent quantum key distribution with vector vortex modes under diverse weather conditions. *Sci. Rep.* **2023**, *13*, 14931. [CrossRef] [PubMed]
122. Klug, A.; Peters, C.; Forbes, A. Robust structured light in atmospheric turbulence. *Adv. Photonics* **2023**, *5*, 016006. [CrossRef]
123. Bai, X.; Wang, Y.; Dai, K. Classification of 270 classes of vector vortex beams using Machine learning-based methods. *Optik* **2023**, *291*, 171362. [CrossRef]
124. Mair, A.; Vaziri, A.; Weihs, G.; Zeilinger, A. Entanglement of the orbital angular momentum states of photons. *Science* **2001**, *412*, 313–316. [CrossRef]
125. Khoury, A.Z.; Souto Ribeiro, P.H.; Dechoum, K. Transfer of angular spectrum in parametric down-conversion with structured light. *Phys. Rev. A* **2020**, *102*, 033708. [CrossRef]
126. Trajtenberg-Mills, S.; Karnieli, A.; Voloch-Bloch, N.; Megidish, E.; Eisenberg, H.S.; Arie, A. Simulating correlations of structured spontaneously down-converted photon pairs. *Laser Photonics Rev.* **2020**, *14*, 1900321. [CrossRef]
127. Rodrigues, R.B.; Alves, G.B.; Barros, R.F.; Souza, C.E.R.; Khoury, A.Z. Generalized orbital angular momentum symmetry in parametric amplification. *Phys. Rev. A* **2022**, *105*, 013510. [CrossRef]
128. Pinheiro da Silva, B.; Buono, W.T.; Pereira, L.J.; Tasca, D.S.; Dechoum, K.; Khoury, A.Z. Spin to orbital angular momentum transfer in frequency up-conversion. *Nanophotonics* **2022**, *11*, 771–778. [CrossRef]
129. Buono, W.T.; Forbes, A. Nonlinear optics with structured light. *Opto-Electron. Adv.* **2022**, *5*, 210174. [CrossRef]
130. Maruca, S.; Kumar, S.; Meng Sua, Y.; Chen, J.Y.; Shahverdi, A.; Huang, Y.P. Quantum Airy photons. *J. Phys. B At. Mol. Opt. Phys.* **2018**, *51*, 175501. [CrossRef]
131. Lib, O.; Bromberg, Y. Spatially entangled Airy photons. *Opt. Lett.* **2020**, *45*, 1399–1402. [CrossRef] [PubMed]
132. Pimenta, R.C.S.; Santos, G.H.d.; Barreto, A.B.; Celeri, L.C.; Ribeiro, P.H.S. Photonic entanglement with accelerated light. *Quantum* **2024**, *8*, 1317. [CrossRef]
133. Gröblacher, S.; Jennewein, T.; Vaziri, A.; Weihs, G.; Zeilinger, A. Experimental quantum cryptography with qutrits. *New J. Phys.* **2006**, *8*, 75. [CrossRef]
134. Mirhosseini, M.; Magaña-Loaiza, O.S.; O'Sullivan, M.N.; Rodenburg, B.; Malik, M.; Lavery, M.P.J.; Padgett, M.J.; Gauthier, D.J.; Boyd, R.W. High-dimensional quantum cryptography with twisted light. *New J. Phys.* **2015**, *17*, 033033. [CrossRef]
135. Mafu, M.; Dudley, A.; Goyal, S.; Giovannini, D.; McLaren, M.; Padgett, M.J.; Konrad, T.; Petruccione, F.; Lütkenhaus, N.; Forbes, A. Higher-dimensional orbital-angular-momentum-based quantum key distribution with mutually unbiased bases. *Phys. Rev. A* **2013**, *88*, 032305. [CrossRef]

136. Fickler, R.; Lapkiewicz, R.; Plick, W.N.; Krenn, M.; Schaeff, C.; Ramelow, S.; Zeilinger, A. Quantum Entanglement of High Angular Momenta. *Science* **2012**, *338*, 640–643. [CrossRef] [PubMed]
137. Fickler, R.; Campbell, G.; Buchlerd, B.; Lamd, P.K.; Zeilinger, A. Quantum entanglement of angular momentum states with quantum numbers up to 10,010. *Proc. Natl. Acad. Sci. USA* **2016**, *113*, 13642–13647. [CrossRef]
138. Stav, T.; Faerman, A.; Maguid, E.; Oren, D.; Kleiner, V.; Hasman, E.; Segev, M. Quantum entanglement of the spin and orbital angular momentum of photons using metamaterials. *Science* **2018**, *361*, 1101–1104. [CrossRef]
139. Nagali, E.; Sciarrino, F. Generation of hybrid polarization-orbital angular momentum entangled states. *Opt. Express* **2010**, *18*, 18243. [CrossRef]
140. Shen, Y.; Rosales-Guzmán, C. Nonseparable states of light: From quantum to classical. *Laser Photonics Rev.* **2022**, *16*, 2100533. [CrossRef]
141. Graffitti, F.; D'Ambrosio, V.; Proietti, M.; Ho, J.; Piccirillo, B.; de Lisio, C.; Marrucci, L.; Fedrizzi, A. Hyperentanglement in structured quantum light. *Phys. Rev. Res.* **2020**, *2*, 043350. [CrossRef]
142. Chen, J.; Qi, G.z.; Wu, Y.; Shi, Y.; Zhao, C.l.; Jin, S.z. Partially coherent twisted vector vortex beam enabling manipulation of high-dimensional classical entanglement. *Opt. Express* **2023**, *31*, 38305. [CrossRef] [PubMed]
143. Wang, J.; Tie, X.; Tan, Z.; Wang, X.; Lei, S.; Wu, P. Recognizing OAM Modes of Electromagnetic Laguerre-Gaussian Schell-Model Vortex Beams in Atmospheric Turbulence from Polarization. *Adv. Quantum Technol.* **2023**, *6*, 2300233. [CrossRef]
144. Hai, L.; Zhang, Z.; Liu, S.; Li, L.; Zhou, Z.; Wang, Q.; Gao, Y.; Gao, C.; Shen, Y.; Fu, S. Intra-Cavity Laser Manipulation of High-Dimensional Non-Separable States. *Laser Photonics Rev.* **2024**, *18*, 2300593. [CrossRef]
145. Kopf, L.; Barros, R.; Fickler, R. Correlating Space, Wavelength, and Polarization of Light: Spatiospectral Vector Beams. *ACS Photonics* **2024**, *11*, 241–246. [CrossRef]
146. Malik, M.; Erhard, M.; Huber, M.; Krenn, M.; Fickler, R.; Zeilinger, A. Multi-photon entanglement in high dimensions. *Nat. Photon.* **2016**, *10*, 248–252. [CrossRef]
147. Wang, X.L.; Luo, Y.H.; Huang, H.L.; Chen, M.C.; Su, Z.E.; Liu, C.; Chen, C.; Li, W.; Fang, Y.Q.; Jiang, X.; et al. 18-Qubit entanglement with six photons' three degrees of freedom. *Phys. Rev. Lett.* **2018**, *120*, 260502. [CrossRef] [PubMed]
148. Krenn, M.; Huber, M.; Fickler, R.; Lapkiewicz, R.; Ramelowa, S.; Zeilinger, A. Generation and confirmation of a (100 × 100)-dimensional entangled quantum system. *Proc. Natl. Acad. Sci. USA* **2014**, *111*, 6243–6247. [CrossRef] [PubMed]
149. Forbes, A.; Nape, I. Quantum mechanics with patterns of light: Progress in high dimensional and multidimensional entanglement with structured light. *AVS Quantum Sci.* **2019**, *1*, 011701. [CrossRef]
150. Gao, X.; Zhang, Y.; D'Errico, A.; Sit, A.; Heshami, K.; Karimi, E. Full Spatial Characterization of Entangled Structured Photons. *Phys. Rev. Lett.* **2024**, *132*, 063802. [CrossRef] [PubMed]
151. Peters, C.; Ornelas, P.; Nape, I.; Forbes, A. Spatially resolving classical and quantum entanglement with structured photons. *Phys. Rev. A* **2023**, *108*, 053502. [CrossRef]
152. Ye, Y.H.; Zeng, L.; Dong, M.X.; Zhang, W.H.; Li, E.Z.; Li, D.C.; Guo, G.C.; Ding, D.S.; Shi, B.S. Long-lived memory for orbital angular momentum quantum states. *Phys. Rev. Lett.* **2022**, *129*, 193601. [CrossRef]
153. Zhou, Z.Q.; Hua, Y.L.; Liu, X.; Chen, G.; Xu, J.S.; Han, Y.J.; Li, C.F.; Guo, G.C. Quantum storage of three-dimensional orbital-angular-momentum entanglement in a crystal. *Phys. Rev. Lett.* **2015**, *115*, 070502. [CrossRef]
154. Fickler, R.; Lapkiewicz, R.; Huber, M.; Lavery, M.P.J.; Padgett, M.J.; Zeilinger, A. Interface between path and orbital angular momentum entanglement for high-dimensional photonic quantum information. *Nat. Commun.* **2014**, *5*, 4502. [CrossRef]
155. Huang, Y.; Li, Y.; Qi, Z.; Feng, J.; Zheng, Y.; Chen, X. A two-way photonic quantum entanglement transfer interface. *Npj Quantum Inf.* **2022**, *8*, 8. [CrossRef]
156. Cozzolino, D.; Bacco, D.; Da Lio, B.; Ingerslev, K.; Ding, Y.; Dalgaard, K.; Kristensen, P.; Galili, M.; Rottwitt, K.; Ramachandran, S.; et al. Orbital angular momentum states enabling fiber-based high-dimensional quantum communication. *Phys. Rev. Appl.* **2019**, *11*, 064058. [CrossRef]
157. Qiu, X.; Zhang, D.; Zhang, W.; Chen, L. Structured-pump-enabled quantum pattern recognition. *Phys. Rev. Lett.* **2019**, *122*, 123901. [CrossRef]
158. Uribe-Patarroyo, N.; Fraine, A.; Simon, D.S.; Minaeva, O.; Sergienko, A.V. Object identification using correlated orbital angular momentum states. *Phys. Rev. Lett.* **2013**, *110*, 043601. [CrossRef]
159. Franke-Arnold, S. Optical angular momentum and atoms. *Philos. Trans. R. Soc. A* **2017**, *375*, 20150435. [CrossRef]
160. Barnett, S.M.; Speirits, F.C.; Babiker, M. Optical angular momentum in atomic transitions: A paradox. *J. Phys. A Math. Theor.* **2022**, *55*, 234008. [CrossRef]
161. Schmiegelow, C.T.; Schulz, J.; Kaufmann, H.; Ruster, T.; Poschinger, U.G.; Schmidt-Kaler, F. Transfer of optical orbital angular momentum to a bound electron. *Nat. Commun.* **2016**, *7*, 12998. [CrossRef]
162. Picón, A.; Benseny, A.; Mompart, J.; Vázquez de Aldana, J.R.; Plaja, L.; Calvo, G.F.; Roso, L. Transferring orbital and spin angular momenta of light to atoms. *New J. Phys.* **2010**, *12*, 083053. [CrossRef]
163. Barnett, S.M.; Berry, M.V. Superweak momentum transfer near optical vortices. *J. Opt.* **2013**, *15*, 125701. [CrossRef]
164. Afanasev, A.; Carlson, C.E.; Mukherjee, A. Superkicks and the photon angular and linear momentum density. *Phys. Rev. A* **2022**, *105*, L061503. [CrossRef]
165. Sola, I.R.; Malinovsky, V.S.; Ahn, J.; Shin, S.; Chang, B.Y. Two-qubit atomic gates: Spatio-temporal control of Rydberg interaction. *Nanoscale* **2023**, *15*, 4325. [CrossRef]

166. Ishihara, J.; Mori, T.; Suzuki, T.; Sato, S.; Morita, K.; Kohda, M.; Ohno, Y.; Miyajima, K. Imprinting spatial helicity structure of vector vortex beam on spin texture in semiconductors. *Phys. Rev. Lett.* **2023**, *130*, 126701. [CrossRef]
167. Andersen, M.F.; Ryu, C.; Cladé, P.; Natarajan, V.; Vaziri, A.; Helmerson, K.; Phillips, W.D. Quantized Rotation of Atoms from Photons with Orbital Angular Momentum. *Phys. Rev. Lett.* **2006**, *97*, 170406. [CrossRef]
168. Wright, K.C.; Leslie, L.S.; Bigelow, N.P. Optical control of the internal and external angular momentum of a Bose-Einstein condensate. *Phys. Rev. A* **2008**, *77*, 041601(R). [CrossRef]
169. Trawi, F.; Billard, F.; Faucher, O.; Béjot, P.; Hertz, E. Molecular Quantum Interface for Storing and Manipulating Ultrashort Optical Vortex. *Laser Photonics Rev.* **2023**, *17*, 2200525. [CrossRef]
170. Verde, M.; Schmiegelow, C.T.; Poschinger, U.; Schmidt-Kaler, F. Trapped atoms in spatially-structured vector light fields. *Sci. Rep.* **2023**, *13*, 21283. [CrossRef]
171. Chen, Y.; Zhou, Y.; Li, M.; Liu, K.; Ciappina, M.F.; Lu, P. Atomic photoionization by spatiotemporal optical vortex pulses. *Phys. Rev. A* **2023**, *107*, 033112. [CrossRef]
172. Berry, M.V.; Dennis, M.R. Quantum cores of optical phase singularities. *J. Opt. A Pure Appl. Opt.* **2004**, *6*, S178–S180. [CrossRef]
173. Barnett, S.M. On the quantum core of an optical vortex. *J. Mod. Opt.* **2014**, *55*, 2279–2292. [CrossRef]
174. Simpson, N.B.; Dholakia, K.; Allen, L.; Padgett, M.J. Mechanical equivalence of spin and orbital angular momentum of light: An optical spanner. *Opt. Lett.* **1997**, *22*, 52–54. [CrossRef] [PubMed]
175. Friese, M.E.J.; Enger, J.; Rubinsztein-Dunlop, H.; Heckenberg, N.R. Optical angular-momentum transfer to trapped absorbing particles. *Phys. Rev. A* **1996**, *54*, 1593–1596. [CrossRef]
176. O'Neil, A.T.; MacVicar, I.; Allen, L.; J, P.M. Intrinsic and Extrinsic Nature of the Orbital Angular Momentum of a Light Beam. *Phys. Rev. Lett.* **2002**, *88*, 053601. [CrossRef] [PubMed]
177. Curtis, J.; Grier, D. Structure of optical vortices. *Phys. Rev. Lett.* **2003**, *90*, 133901. [CrossRef] [PubMed]
178. Garcés-Chávez, V.; McGloin, D.; Padgett, M.J.; Dultz, W.; Schmitzer, H.; Dholakia, K. Observation of the Transfer of the Local Angular Momentum Density of a Multiringed Light Beam to an Optically Trapped Particle. *Phys. Rev. Lett.* **2003**, *91*, 103601. [CrossRef]
179. Li, M.; Yan, S.; Yao, B.; Liang, Y.; Zhang, P. Spinning and orbiting motion of particles in vortex beams with circular or radial polarizations. *Opt. Express* **2016**, *24*, 20604–20612. [CrossRef]
180. Babiker, M.; Andrews, D.L.; Lembessis, V.E. Atoms in complex twisted light. *J. Opt.* **2019**, *21*, 013001. [CrossRef]
181. Ng, J.; Lin, Z.; Chan, C.T. Theory of Optical Trapping by an Optical Vortex Beam. *Phys. Rev. Lett.* **2010**, *104*, 103601. [CrossRef] [PubMed]
182. Yang, Y.; Ren, Y.X.; Chen, M.; Arita, Y.; Rosales-Guzmán, C. Optical trapping with structured light: A review. *Adv. Photonics* **2021**, *3*, 034001. [CrossRef]
183. Li, M.; Yan, S.; Zhang, Y.; Zhou, Y.; Yao, B. Orbital angular momentum in optical manipulations. *J. Opt.* **2022**, *24*, 114001. [CrossRef]
184. Padgett, M.; Bowman, R. Tweezers with a twist. *Nat. Photonics* **2011**, *5*, 243–248. [CrossRef]
185. Stickler, B.A.; Hornberger, K.; Kim, M.S. Quantum rotations of nanoparticles. *Nat. Rev.* **2021**, *3*, 589–597. [CrossRef]
186. Stickler, B.A.; Papendell, B.; Kuhn, S.; Schrinski, B.; Millen, J.; Arndt, M.; Hornberger, K. Probing macroscopic quantum superpositions with nanorotors. *New J. Phys.* **2018**, *20*, 122001. [CrossRef]
187. Zhao, R.; Manjavacas, A.; García de Abajo, F.J.; Pendry, J.B. Rotational Quantum Friction. *Phys. Rev. Lett.* **2012**, *109*, 123604. [CrossRef]
188. Wood, A.A.; Hollenberg, L.C.L.; Scholten, R.E.; Martin, A.M. Observation of a Quantum Phase from Classical Rotation of a Single Spin. *Phys. Rev. Lett.* **2020**, *124*, 020401. [CrossRef] [PubMed]
189. Hu, Y.; Kingsley-Smith, J.J.; Nikkhou1, M.; Sabin, J.A.; Rodríguez-Fortuño, F.J.; Xu, X.; Millen, J. Structured transverse orbital angular momentum probed by a levitated optomechanical sensor. *Nat. Commun.* **2023**, *14*, 2638. [CrossRef]
190. Li, C.; Jang, J.; Badloe, T.; Yang, T.; Kim, J.; Kim, J.; Nguyen, M.; Maier, S.A.; Rho, J.; Ren, H.; et al. Arbitrarily structured quantum emission with a multifunctional metalens. *eLight* **2023**, *3*, 19. [CrossRef]
191. Liang, H.; Ahmed, H.; Tam, W.Y.; Chen, X.; Li, J. Continuous heralding control of vortex beams using quantum metasurface. *Commun. Phys.* **2023**, *6*, 140. [CrossRef]
192. Liu, X.; Kan, Y.; Kumar, S.; Kulikova, L.F.; Davydov, V.A.; Agafonov, V.N.; Zhao, C.; Bozhevolnyi, S.I. Ultracompact Single-Photon Sources of Linearly Polarized Vortex Beams. *Adv. Mater.* **2024**, *36*, 2304495. [CrossRef]
193. Li, Z.; Guo, H.; Liu, H.; Li, J.; Sun, H.; Yang, R.; Liu, K.; Gao, J. Higher-order spatially squeezed beam for enhanced spatial measurements. *Adv. Quantum Technol.* **2022**, *5*, 2200055. [CrossRef]
194. Heinze, J.; Willke, B.; Vahlbruch, H. Observation of squeezed states of light in higher-order Hermite-Gaussian modes with a quantum noise reduction of up to 10 dB. *Phys. Rev. Lett.* **2022**, *128*, 083606. [CrossRef]
195. Goldberg, A.Z.; de la Hoz, P.; Björk, G.; Klimov, A.B.; Grassl, M.; Leuchs, G.; Sánchez-Soto, L.L. Quantum concepts in optical polarization. *Adv. Opt. Photonics* **2021**, *13*, 1–73. [CrossRef]
196. Yang, L.P.; Jacob, Z. Non-classical photonic spin texture of quantum structured light. *Commun. Phys.* **2021**, *4*, 221. [CrossRef]
197. Andrews, D.L. Symmetry and quantum features in optical vortices. *Symmetry* **2021**, *13*, 1368. [CrossRef]
198. Williams, M.D.; Bradshaw, D.S.; Andrews, D.L. Quantum issues with structured light. *Proc. SPIE* **2016**, *9764*, 976407. [CrossRef]

199. Smith, B.J.; Raymer, M.G. Photon wave functions, wave-packet quantization of light, and coherence theory. *New J. Phys.* **2007**, *9*, 414. [CrossRef]
200. Bialynicki-Birula, I.; Bialynicka-Birula, Z. Quantum numbers and spectra of structured light. *Phys. Scr.* **2018**, *93*, 104005. [CrossRef]
201. Bialynicki-Birula, I. Helicity amplitudes, polarization of EM waves and Stokes parameters: Classical versus quantum theory. *J. Opt.* **2019**, *21*, 094002. [CrossRef]
202. Nienhuis, G. Analogies between optical and quantum mechanical angular momentum. *Philos. Trans. R. Soc. A* **2017**, *375*, 20150443. [CrossRef]
203. Sugic, D.; Droop, R.; Otte, E.; Ehrmanntraut, D.; Nori, F.; Ruostekoski, J.; Denz, C.; Dennis, M.R. Particle-like topologies in light. *Nat. Commun.* **2021**, *12*, 6785. [CrossRef] [PubMed]
204. Shen, Y.; Zhang, Q.; Shi, P.; Du, L.; Yuan, X.; Zayats, A.V. Optical skyrmions and other topological quasiparticles of light. *Nat. Photon.* **2024**, *18*, 15–25. [CrossRef]
205. Tamburini, F.; Thidé, B.; Licata, I.; Bouchard, F.; Karimi, E. Majorana bosonic quasiparticles from twisted photons in free space. *Phys. Rev. A* **2021**, *103*, 033505. [CrossRef]
206. Li, Z.X.; Ruan, Y.P.; Tang, J.; Liu, Y.; Liu, J.J.; Tang, J.S.; Zhang, H.; Xia, K.Y.; Lu, Y.Q. Self-healing of a heralded single-photon Airy beam. *Opt. Express* **2021**, *29*, 40187. [CrossRef]
207. Nape, I.; Otte, E.; Vallés, A.; Rosales-Guzmán, C.; Cardano, F.; Denz, C.; Forbes, A. Self-healing high-dimensional quantum key distribution using hybrid spin-orbit Bessel states. *Opt. Express* **2018**, *26*, 26946. [CrossRef]
208. McLaren, M.; Mhlanga, T.; Padgett, M.J.; Roux, F.S.; Forbes, A. Self-healing of quantum entanglement after an obstruction. *Nat. Commun.* **2014**, *5*, 3248. [CrossRef]
209. Yang, D.; Yu, Z.; Wang, W.; Hu, Z.D.; Zhu, Y. Underwater entanglement propagation of auto-focusing Airy beams. *Opt. Express* **2024**, *32*, 4887. [CrossRef]
210. Giovannini, D.; Romero, J.; Potoček, V.; Ferenczi, G.; Speirits, F.; Barnett, S.M.; Faccio, D.; Padgett, M.J. Spatially structured photons that travel in free space slower than the speed of light. *Science* **2015**, *347*, 857–860. [CrossRef]
211. Petrov, N.I. Speed of structured light pulses in free space. *Sci. Rep.* **2019**, *9*, 18332. [CrossRef]
212. Silenko, A.J.; Zhang, P.; Zou, L. Relativistic quantum-mechanical description of twisted paraxial electron and photon beams. *Phys. Rev. A* **2019**, *100*, 030101(R). [CrossRef]
213. Shen, Y.; Nape, I.; Yang, X.; Fu, X.; Gong, M.; Naidoo, D.; Forbes, A. Creation and control of high-dimensional multi-partite classically entangled light. *Light Sci. Appl.* **2021**, *10*, 50. [CrossRef] [PubMed]
214. Wan, Z.; Wang, Z.; Yang, X.; Shen, Y.; Fu, X. Digitally tailoring arbitrary structured light of generalized ray-wave duality. *Opt. Express* **2020**, *28*, 31043. [CrossRef] [PubMed]
215. Shen, Y.; Zdagkas, A.; Papasimakis, N.; Zheludev, N.I. Measures of space-time nonseparability of electromagnetic pulses. *Phys. Rev. Res.* **2021**, *3*, 013236. [CrossRef]
216. Gomes, R.M.; Salles, A.; Toscano, F.; Souto Ribeiro, P.H.; Walborn, S.P. Observation of a nonlocal optical vortex. *Phys. Rev. Lett.* **2009**, *103*, 033602. [CrossRef]
217. Qi, W.R.; Liu, R.; Kong, L.J.; Wang, Z.X.; Huang, S.Y.; Tu, C.; Li, Y.; Wang, H.T. Double-slit interference of single twisted photons. *Chin. Opt. Lett.* **2020**, *18*, 102601. [CrossRef]
218. Aili, M.; Liu, P.; Chen, X.X.; Wu, Q.Y.; Meng, Z.; Yang, J.Z.; Li, J.; Zhang, A.N. Double-slit experiment with multiple vortex beams. *Phys. Rev. A* **2024**, *109*, 013521. [CrossRef]
219. Franke-Arnold, S.; Barnett, S.M.; Yao, E.; Leach, J.; Courtial, J.; Padgett, M. Uncertainty principle for angular position and angular momentum. *New J. Phys.* **2004**, *6*, 103. [CrossRef]
220. Gounden, N.; Epstein, J.; Ornelas, P.; Beck, G.; Nape, I.; Forbes, A. Popper's conjecture with angular slits and twisted light. *Sci. Rep.* **2023**, *13*, 21701. [CrossRef]
221. Nape, I.; Ndagano, B.; Forbes, A. Erasing the orbital angular momentum information of a photon. *Phys. Rev. A* **2017**, *95*, 053859. [CrossRef]
222. Zhang, Y.; Agnew, M.; Roger, T.; Roux, F.S.; Konrad, T.; Faccio, D.; Leach, J.; Forbes, A. Simultaneous entanglement swapping of multiple orbital angular momentum states of light. *Nat. Commun.* **2017**, *8*, 632. [CrossRef]
223. Liu, S.; Lou, Y.; Jing, J. Orbital angular momentum multiplexed deterministic all-optical quantum teleportation. *Nat. Commun.* **2020**, *11*, 3875. [CrossRef]
224. Wang, X.L.; Cai, X.D.; Su, Z.E.; Chen, M.C.; Wu, D.; Li, L.; Liu, N.L.; Lu, C.Y.; Pan, J.W. Quantum teleportation of multiple degrees of freedom of a single photon. *Nature* **2015**, *518*, 516–519. [CrossRef] [PubMed]
225. Zhang, Y.; Roux, F.S.; Konrad, T.; Agnew, M.; Leach, J.; Forbes, A. Engineering two-photon high-dimensional states through quantum interference. *Sci. Adv.* **2016**, *2*, e1501165. [CrossRef]
226. Kevin, S.; Sahrai, M.; Asadpour, S.H. Controllable Hartman effect by vortex beam in a one dimensional photonic crystal doped by graphene quantum dots. *Sci. Rep.* **2023**, *13*, 2992. [CrossRef]
227. Leach, J.; Jack, B.; Romero, J.; Ritsch-Marte, M.; Boyd, R.W.; Jha, A.K.; Barnett, S.M.; Franke-Arnold, S.; Padgett, M.J. Violation of a Bell inequality in two-dimensional orbital angular momentum state-spaces. *Opt. Express* **2009**, *17*, 8287–8293. [CrossRef]
228. Romero, J.; Leach, J.; Jack, B.; Barnett, S.M.; Padgett, M.J.; Franke-Arnold, S. Violation of Leggett inequalities in orbital angular momentum subspaces. *New J. Phys.* **2010**, *12*, 123007. [CrossRef]

229. Dada, A.; Leach, J.; Buller, G.S.; Padgett, M.J.; Andersson, E. Experimental high-dimensional two-photon entanglement and violations of generalized Bell inequalities. *Nat. Phys.* **2011**, *7*, 677–680. [CrossRef]
230. Tang, Y.; Perrie, W.; Schille, J.; Loeschner, U.; Li, Q.; Liu, D.; Edwardson, S.P.; Forbes, A.; Dearden, G. High-quality vector vortex arrays by holographic and geometric phase control. *J. Phys. D Appl. Phys.* **2020**, *53*, 465101. [CrossRef]
231. Qi, W.R.; Zhou, J.; Kong, L.J.; Xu, Z.P.; Meng, H.X.; Liu, R.; Wang, Z.X.; Tu, C.; Li, Y.L.; Cabello, A.; et al. Stronger Hardy-like proof of quantum contextuality. *Photonics Res.* **2022**, *10*, 1582–1593. [CrossRef]
232. Karimi, E.; Leach, J.; Slussarenko, S.; Piccirillo, B.; Marrucci, L.; Chen, L.; She, W.; Franke-Arnold, S.; Padgett, M.J.; Santamato, E. Spin-orbit hybrid entanglement of photons and quantum contextuality. *Phys. Rev. A* **2010**, *82*, 022115. [CrossRef]
233. Xu, J.M.; Zhen, Y.Z.; Yang, Y.X.; Cheng, Z.M.; Ren, Z.C.; Chen, K.; Wang, X.L.; Wang, H.T. Experimental Demonstration of Quantum Pseudotelepathy. *Phys. Rev. Lett.* **2022**, *129*, 050402. [CrossRef]
234. Leach, J.; Jack, B.; Romero, J.; Jha, A.K.; Yao, A.M.; Franke-Arnold, S.; Ireland, D.G.; Boyd, R.W.; Barnett, S.M.; Padgett, M.J. Quantum correlations in optical angle-orbital angular momentum variables. *Science* **2010**, *329*, 662–665. [CrossRef] [PubMed]
235. Slussarenko, S.; Joch, D.J.; Tischler, N.; Ghafari, F.; Shalm, L.K.; Verma, V.B.; Nam, S.W.; Pryde, G.J. Quantum steering with vector vortex photon states with the detection loophole closed. *Npj Quantum Inf.* **2022**, *8*, 20. [CrossRef]
236. Stoklasa, B.; Motka, L.; Rehacek, J.; Hradil, Z.; Sánchez-Soto, L.L.; Agarwal, G.S. Experimental violation of a Bell-like inequality with optical vortex beams. *New J. Phys.* **2015**, *17*, 113046. [CrossRef]
237. González-Domínguez, M.A.; Piceno-Martínez, A.E.; Rosales-Zárate, L.E.C. Nonlocality and quantum correlations in Ince–Gauss structured light modes. *J. Opt. Soc. Am. B* **2023**, *40*, 881. [CrossRef]
238. Prevedel, R.; Cronenberg, G.; Tame, M.S.; Paternostro, M.; Walther, P.; Kim, M.S.; Zeilinger, A. Experimental realization of Dicke states of up to six qubits for multiparty quantum networking. *Phys. Rev. Lett.* **2009**, *103*, 020503. [CrossRef]
239. Erhard, M.; Malik, M.; Krenn, M.; Zeilinger, A. Experimental Greenberger-Horne-Zeilinger entanglement beyond qubits. *Nat. Photon* **2018**, *12*, 759–764. [CrossRef]
240. Wang, F.; Erhard, M.; Babazadeh, A.; Malik, M.; Krenn, M.; Zeilinger, A. Generation of the complete four-dimensional Bell basis. *Optica* **2017**, *4*, 1462. [CrossRef]
241. Kong, L.J.; Li, Y.; Liu, R.; Qi, W.R.; Wang, Q.; Wang, Z.X.; Huang, S.Y.; Si, Y.; Tu, C.; Hu, W.; et al. Complete measurement and multiplexing of orbital angular momentum Bell states. *Phys. Rev. A* **2019**, *100*, 023822. [CrossRef]
242. Wang, Y.; Ru, S.; Wang, F.; Zhang, P.; Li, F. Experimental demonstration of efficient high-dimensional quantum gates with orbital angular momentum. *Quantum Sci. Technol.* **2022**, *7*, 015016. [CrossRef]
243. Babazadeh, A.; Erhard, M.; Wang, F.; Malik, M.; Nouroozi, R.; Krenn, M.; Zeilinger, A. High-dimensional single-photon quantum gates: Concepts and experiments. *Phys. Rev. Lett.* **2017**, *119*, 180510. [CrossRef] [PubMed]
244. Vashukevich, E.A.; Bashmakova, E.N.; Golubeva, T.Y.; Golubev, Y.M. High-fidelity quantum gates for OAM single qudits on quantum memory. *Laser Phys. Lett.* **2022**, *19*, 025202. [CrossRef]
245. Bashmakova, E.N.; Vashukevich, E.A.; Golubeva, T.Y. Parallel multi-two-qubit swap gate via quantum nondemolition interaction of orbital-angular-momentum light and an atomic ensemble. *Phys. Rev. A* **2024**, *109*, 012428. [CrossRef]
246. Nape, I.; Sephton, B.; Ornelas, P.; Moodley, C.; Forbes, A. Quantum structured light in high dimensions. *APL Photonics* **2023**, *8*, 051101. [CrossRef]
247. Eriksson, M.; Goldberg, A.; Hiekkamäki, M.; Bouchard, F.; Rehacek, J.; Hradil, Z.; Leuchs, G.; Fickler, R.; Sánchez-Soto, L. Sensing Rotations with Multiplane Light Conversion. *Phys. Rev. Appl.* **2023**, *20*, 024052. [CrossRef]
248. Jayaseelan, M.; Murphree, J.D.; Schultz, J.T.; Ruostekoski, J.; Bigelow, N.P. Topological atom optics and beyond with knotted quantum wavefunctions. *Commun Phys* **2024**, *7*, 7. [CrossRef]
249. Aharonov, Y.; Albert, D.Z.; Vaidman, L. How the result of a measurement of a component of the spin of a spin-1/2 particle can turn out to be 100. *Phys. Rev. Lett.* **1988**, *60*, 1351–1354. [CrossRef]
250. Dressel, J.; Malik, M.; Miatto, F.M.; Jordan, A.N.; Boyd, R.W. Colloquium: Understanding quantum weak values: Basics and applications. *Rev. Mod. Phys.* **2013**, *86*, 307–316. [CrossRef]
251. Forbes, A. Structured light from lasers. *Laser Photonics Rev.* **2019**, *13*, 1900140. [CrossRef]
252. Resch, K.J.; Lundeen, J.S.; Steinberg, A.M. Experimental realization of the quantum box problem. *Phys. Lett.* **2004**, *324*, 125–131. [CrossRef]
253. Ashby, J.M.; Schwarz, P.D.; Schlosshauer, M. Observation of the quantum paradox of separation of a single photon from one of its properties. *Phys. Rev. A* **2016**, *94*, 012102. [CrossRef]
254. Kumar Pan, A. Disembodiment of arbitrary number of properties in quantum Cheshire cat experiment. *Eur. Phys. J. D* **2020**, *74*, 151. [CrossRef]
255. Kocsis, S.; Braverman, B.; Ravets, S.; Stevens, M.J.; Mirin, R.P.; Shalm, L.K.; Steinberg, A.M. Observing the average trajectories of single photons in a two-slit interferometer. *Science* **2011**, *332*, 1170–1173. [CrossRef]
256. Bliokh, K.Y.; Bekshaev, A.Y.; Kofman, A.G.; Nori, F. Photon trajectories, anomalous velocities and weak measurements: A classical interpretation. *New J. Phys.* **2013**, *15*, 073022. [CrossRef]
257. Li, Y.; Ren, Z.C.; Kong, L.J.; Tu, C.; Wang, H.T. Trajectory-based unveiling of the angular momentum of photons. *Phys. Rev. A* **2017**, *95*, 043830. [CrossRef]
258. Berry, M.V. Optical currents. *J. Opt. A: Pure Appl. Opt.* **2009**, *11*, 094001. [CrossRef]

259. Berry, M.V. Quantum backflow, negative kinetic energy, and optical retro-propagation. *J. Phys. A Math. Theor.* **2010**, *43*, 415302. [CrossRef]
260. Ghosh, B.; Daniel, A.; Gorzkowski, B.; Lapkiewicz, R. Azimuthal backflow in light carrying orbital angular momentum. *Optica* **2023**, *10*, 1217. [CrossRef]
261. Lundeen, J.S.; Sutherland, B.; Patel, A.; Stewart, C.; Bamber, C. Direct measurement of the quantum wavefunction. *Nature* **2011**, *474*, 188–191. [CrossRef] [PubMed]
262. Malik, M.; Mirhosseini, M.; Lavery, M.P.J.; Leach, J.; Padgett, M.J.; Boyd, R.W. Direct measurement of a 27-dimensional orbital-angular-momentum state vector. *Nat. Commun.* **2014**, *5*, 3115. [CrossRef]
263. Shi, Z.; Mirhosseini, M.; Margiewicz, J.; Malik, M.; Rivera, F.; Zhu, Z.; Boyd, R.W. Scan-free direct measurement of an extremely high-dimensional photonic state. *Optica* **2015**, *2*, 388–392. [CrossRef]
264. Mirhosseini, M.; Lundeen, J.S.; Boyd, R.W. Direct measurement of the photon's spatial wave function. In *Quantum Photonics: Pioneering Advances and Emerging Applications*; Springer Nature Switzerland AG: Cham, Switzerland, 2019; pp. 25–49. [CrossRef]
265. Zhang, C.R.; Hu, M.J.; Hou, Z.B.; Tang, J.F.; Zhu, J.; Xiang, G.Y.; Li, C.F.; Guo, G.C.; Zhang, Y.S. Direct measurement of the two-dimensional spatial quantum wave function via strong measurements. *Phys. Rev. A* **2020**, *101*, 012119. [CrossRef]
266. Zhang, C.R.; Hu, M.J.; Xiang, G.Y.; Zhang, Y.S.; Li, C.F.; Guo, G.C. Direct strong measurement of a high-dimensional quantum state. *Chin. Phys. Lett.* **2020**, *37*, 080301. [CrossRef]
267. Yang, M.; Xiao, Y.; Liao, Y.W.; Liu, Z.H.; Xu, X.Y.; Xu, J.S.; Li, C.F.; Guo, G.C. Zonal reconstruction of photonic wavefunction via momentum weak measurement. *Laser Photonics Rev.* **2020**, *14*, 1900251. [CrossRef]
268. de Lima Bernardo, B.; Azevedo, S.; Rosas, A. Simplified algebraic description of weak measurements with Hermite-Gaussian and Laguerre-Gaussian pointer states. *Opt. Commun.* **2014**, *331*, 194–197. [CrossRef]
269. Turek, Y.; Kobayashi, H.; Akutsu, T.; Sun, C.P.; Shikano, Y. Post-selected von Neumann measurement with Hermite-Gaussian and Laguerre-Gaussian pointer states. *New J. Phys.* **2015**, *17*, 083029. [CrossRef]
270. Kobayashi, H.; Nonaka, K.; Shikano, Y. Stereographical visualization of a polarization state using weak measurements with an optical-vortex beam. *Phys. Rev. A* **2014**, *89*, 053816. [CrossRef]
271. Tukiainen, M.; Kobayashi, H.; Shikano, Y. Quantification of concurrence via weak measurement. *Phys. Rev. A* **2017**, *95*, 052301. [CrossRef]
272. Xia, B.; Huang, J.; Li, H.; Liu, M.; Xiao, T.; Chen, F.; Zeng, G. Ultrasensitive measurement of angular rotations via a Hermite-Gaussian pointer. *Photonics Res.* **2022**, *10*, 2816–2827. [CrossRef]
273. Xia, B.; Huang, J.; Fang, C.; Li, H.; Zeng, G. High-precision multiparameter weak measurement with Hermite-Gaussian pointer. *Phys. Rev. Appl.* **2020**, *13*, 034023. [CrossRef]
274. Magaña-Loaiza, O.S.; Mirhosseini, M.; Rodenburg, B.; Boyd, R.W. Amplification of angular rotations using weak measurements. *Phys. Rev. Lett.* **2014**, *112*, 200401. [CrossRef]
275. Resch, K.J.; Steinberg, A.M. Extracting joint weak values with local, single-particle measurements. *Phys. Rev. Lett.* **2004**, *92*, 130402. [CrossRef]
276. Kobayashi, H.; Puentes, G.; Shikano, Y. Extracting joint weak values from two-dimensional spatial displacements. *Phys. Rev. A* **2012**, *86*, 053805. [CrossRef]
277. Zhu, W.; Zhang, S.; Liang, X.; Zheng, H.; Zhong, Y.; Yu, J.; Chen, Z.; Zhang, L. Joint spatial weak measurement with higher-order Laguerre-Gaussian point states. *Opt. Express* **2022**, *30*, 17848–17857. [CrossRef]
278. Puentes, G.; Hermosa, N.; Torres, J.P. Weak measurements with orbital-angular-momentum pointer states. *Phys. Rev. Lett.* **2012**, *109*, 040401. [CrossRef]
279. Qiu, J.; Ren, C.; Zhang, Z. Precisely measuring the orbital angular momentum of beams via weak measurement. *Phys. Rev. A* **2016**, *93*, 063841. [CrossRef]
280. Zhu, J.; Zhang, P.; Li, Q.; Wang, F.; Wang, C.; Zhou, Y.; Wang, J.; Gao, H.; Kwek, L.C.; Li, F. Measuring the topological charge of orbital angular momentum beams by utilizing weak measurement principle. *Sci. Rep.* **2019**, *9*, 7993. [CrossRef] [PubMed]
281. Cormann, M.; Caudano, Y. Geometric description of modular and weak values in discrete quantum systems using the Majorana representation. *J. Phys. A Math. Theor.* **2017**, *50*, 305302. [CrossRef]
282. Ballesteros Ferraz, L.; Lambert, D.L.; Caudano, Y. Geometrical interpretation of the argument of weak values of general observables in N-level quantum systems. *Quantum Sci. Technol.* **2022**, *7*, 045028. [CrossRef]
283. Cormann, M.; Remy, M.; Kolaric, B.; Caudano, Y. Revealing geometric phases in modular and weak values with a quantum eraser. *Phys. Rev. A* **2016**, *93*, 042124. [CrossRef]
284. Wang, B.; Li, P.; Chen, T.; Zhang, X. Accurately identifying mode indices of Laguerre-Gaussian beams via weak measurements. *J. Opt.* **2017**, *19*, 055603. [CrossRef]
285. Zhu, J.; Zhang, P.; Wang, F.; Wang, Y.; Li, Q.; Liu, R.; Wang, J.; Gao, H.; Li, F. Experimentally measuring the mode indices of Laguerre-Gaussian beams by weak measurement. *Opt. Express* **2021**, *29*, 5419–5426. [CrossRef]
286. Wang, A.; Zhu, J.; Luo, L.; Liu, X.; Ye, L.; Zhang, Z.; Du, J. Optical differentiation based on weak measurements. *Opt. Lett.* **2022**, *47*, 3880. [CrossRef]
287. Fang, L.; Luo, L.; Zhao, R.; Liu, B. Measuring the Orbital Angular Momentum of Light Based on Optical Differentiation. *IEEE Photonics J.* **2023**, *15*, 1–7. [CrossRef]
288. Bliokh, Y.K.; Aiello, A. Goos-Hänchen and Imbert-Fedorov beam shifts: An overview. *J. Opt.* **2013**, *15*, 014001. [CrossRef]

289. Hosten, O.; Kwiat, P. Observation of the spin Hall effect of light via weak measurements. *Science* **2008**, *319*, 787–790. [CrossRef]
290. Jayaswal, G.; Mistura, G.; Merano, M. Weak measurement of the Goos–Hänchen shift. *Opt. Lett.* **2013**, *38*, 1232–1234. [CrossRef]
291. Jayaswal, G.; Mistura, G.; Merano, M. Observing angular deviations in light-beam reflection via weak measurements. *Opt. Lett.* **2014**, *39*, 6257–6260. [CrossRef]
292. Goswami, S.; Pal, M.; Nandi, A.; Panigrahi, P.K.; Ghosh, N. Simultaneous weak value amplification of angular Goos-Hänchen and Imbert-Fedorov shifts in partial reflection. *Opt. Lett.* **2014**, *39*, 6229–6232. [CrossRef]
293. Prajapati, C.; Viswanathan, N.K. Simultaneous weak measurement of angular and spatial Goos-Hänchen and Imbert-Fedorov shifts. *J. Opt.* **2017**, *19*, 105611. [CrossRef]
294. Dennis, M.R.; Götte, J.B. The analogy between optical beam shifts and quantum weak measurements. *New J. Phys.* **2012**, *14*, 073013. [CrossRef]
295. Dennis, M.R.; Götte, J.B. Beam shifts to reflected light beams and their axial structure. *Proc. SPIE* **2014**, *9441*, 94410M. [CrossRef]
296. Merano, M.; Hermosa, N.; Woerdman, J.P.; Aiello, A. How orbital angular momentum affects beam shifts in optical reflection. *Phys. Rev. A* **2010**, *82*, 023817. [CrossRef]
297. Zhang, X.; Wang, S.; Liu, J.; Wu, J.; Li, J. Spin-Hall Effect of Cylindrical Vector Vortex Beams. *Photonics* **2023**, *10*, 1356. [CrossRef]
298. Long, W.; Pan, J.; Guo, X.; Liu, X.; Lin, H.; Zheng, H.; Yu, J.; Guan, H.; Lu, H.; Zhong, Y.; et al. Optimized weak measurement of orbital angular momentum-induced beam shifts in optical reflection. *Photonics Res.* **2019**, *7*, 1273–1278. [CrossRef]
299. Mandal, S.; Das, A.; Pradhan, M. Weak measurement of the Goos–Hänchen shift for a Hermite–Gaussian laser beam. *J. Opt.* **2024**, *26*, 045403. [CrossRef]
300. Prajapati, C.; Viswanathan, N.K. Enhancement of weak spin-Hall shift using higher-order helical-wavefront beams. *OSA Contin.* **2018**, *1*, 872–881. [CrossRef]
301. Xie, S.; Zhu, J.; Wang, A.; Wang, Y.; Huang, Y.; Zhang, Z. Super amplification enabled by orbital angular momentum in weak measurement. *Opt. Express* **2024**, *32*, 11794. [CrossRef]
302. Töppel, F.; Ornigotti, M.; Aiello, A. Goos-Hänchen and Imbert-Fedorov shifts from a quantum-mechanical perspective. *New J. Phys.* **2013**, *15*, 113059. [CrossRef]
303. Shi, L.k.; Song, J.C.W. Shift vector as the geometric origin of beam shifts. *Phys. Rev. B* **2019**, *100*, 201405(R). [CrossRef]
304. Xu, L.; Liu, Z.; Datta, A.; Knee, G.C.; Lundeen, J.S.; Lu, Y.Q.; Zhang, L. Approaching quantum-limited metrology with imperfect detectors by using weak-value amplification. *Phys. Rev. Lett.* **2020**, *125*, 080501. [CrossRef]
305. Yin, X.; Hesselink, L. Goos-Hänchen shift surface plasmon resonance sensor. *Appl. Phys. Lett.* **2006**, *89*, 261108. [CrossRef]
306. Wang, X.; Yin, C.; Sun, J.; Li, H.; Wang, Y.; Ran, M.; Cao, Z. High-sensitivity temperature sensor using the ultrahigh order mode-enhanced Goos-Hänchen effect. *Opt. Express* **2013**, *11*, 13380. [CrossRef]
307. Xu, L.; Luo, L.; Wu, H.; Luo, Z.; Zhang, Z.; Shi, H.; Chang, T.; Wu, P.; Du, C.; Cui, H.L. Measurement of chiral molecular parameters based on a combination of surface plasmon resonance and weak value amplification. *ACS Sens.* **2020**, *5*, 2398–2407. [CrossRef] [PubMed]
308. Tang, T.; Shen, K.; Li, J.; Liang, X.; Tang, Y.; Li, C.; He, Y. Optimal weak measurement scheme for chiral molecular detection based on photonic spin Hall effect. *Opt. Express* **2023**, *31*, 40308. [CrossRef]
309. Wang, Y.; Yang, S.; Zhang, Q.; Chen, Y.; Hu, X.; Zhang, H.; Zhang, Z. Complete chiroptical signal detection using weak measurement with intensity-contrast-ratio pointers. *APL Photonics* **2023**, *8*, 126102. [CrossRef]